

Chalmers University of Technology

60GHz Contactless Transition from Microstrip to Gap Waveguide Suitable for Packaging and Integration of RF MMIC with Gap Waveguide Antenna

Master's thesis in Wireless Photonics and Space Engineering

Uttam Nandi

MASTER'S THESIS 2016

**60GHz Contactless Transition from Microstrip to
Gap Waveguide Suitable for Packaging and
Integration of RF MMIC with Gap Waveguide
Antenna**

UTTAM NANDI



CHALMERS
UNIVERSITY OF TECHNOLOGY

Department of Signals and Systems
Division of Antenna Systems
CHALMERS UNIVERSITY OF TECHNOLOGY
Gothenburg, Sweden 2016

© Uttam Nandi, 2016.

Supervisor: Ashraf Uz Zaman, Assistant Professor, Signals and System
Examiner: Jian Yang, Associate Professor, Signal and Systems

Master's Thesis 2016
Department of Signals and Systems
Division of Antenna Systems
Chalmers University of Technology
SE-412 96 Gothenburg
Telephone +46 31 772 1000

Printed by [Chalmers Library]
Gothenburg, Sweden 2016

Uttam Nandi
Wireless Photonics and Space Engineering
Department of Signals and Systems
Chalmers University of Technology

Abstract

The demand for high-speed data connectivity and high resolution video transfer is leading to huge data traffic in wireless network and hence there is a growing interest in utilizing the millimeter wave frequency band for communication purpose. However, several issues like high path loss and low penetrating capacity of millimeter waves, and losses at circuit interconnects limits the extensive use of millimeter waves for communication. In this project techniques to make contactless transitions from Microstrip to Gap Waveguide (Ridge and Groove) have been investigated. Transition from Microstrip to Gap Waveguide can be used for packaging and for integration of MMIC chips with Gap Waveguide array antennas. Such integration will enable amplitude and phase control on each antenna sub-array and hence beam steering. It will also make the millimeter wave Tx/Rx module compact and can also be utilised for massive MIMO. Compact Tx/Rx module, beam steering and massive MIMO are some of the key features required for utilizing millimeter waves for communication.

In this thesis a new technique to make back to back transitions from Microstrip to Gap Waveguide (Ridge and Groove) has been proposed. The proposed transition method has been simulated in CST and the final prototypes has been fabricated to experimentally verify the results. This technique is universal and can also be used to make rectangular waveguide-microstrip and microstrip-microstrip transitions. Hence, it has great potential in various applications, such as replacing old traditional transition methods like bond wire and flip chip. Optimization of the transitions for Microstrip to Gap Waveguide (Ridge and Groove) has been done using Roger 3010 with $\epsilon_r = 10.2$ (close to that of MMIC substrate). The back to back transition from Microstrip to Ridge gap waveguide had a bandwidth of 21.14%. Transition from Microstrip to Groove gap waveguide also had 21.14% bandwidth however with some smart modification in the transition 27.2% bandwidth has been achieved. The manufactured prototypes and PCBs were made by brass and alumina ($\epsilon_r = 9.9$) respectively. Despite the less tolerance level for manufacturing the prototypes the measured results were in acceptable limits to validate the working of this kind of transitions.

Keywords: Gap Waveguide, Ridge Gap Waveguide (RGW), Groove Gap Waveguide (GGW), Rectangular waveguide (RW), Microstrip Line, Coplanar Line, monolithic microwave integrated circuit (MMIC).

Acknowledgements

Firstly I would like to thank the late Prof. Per-Simon Kildal who was a big source of inspiration for me to do my master thesis in the Antenna Department. His absence will be felt in my thesis presentation and even thereafter. Secondly I would like to thank my supervisor Ashraf Uz Zaman who guided me on a regular basis. He was monitoring my work and giving me feedback and ideas on a daily basis no matter how busy he was. I would also like to thank my examiner Jian Yang with whom we have had meetings at least once a week and discuss on how to proceed with the thesis. Next I would like to thank Phd student Abbas who helped me to learn CST and provide me with useful knowledge which I needed to proceed with my work. Abbas and Jinlin were really very nice and friendly and created a very good environment to work in. Lastly I would like to thank my parents who have supported me emotionally and financially throughout my stay in Sweden.

Uttam Nandi, Gothenburg, June 2016

Contents

List of Figures	xi
List of Tables	xv
1 Introduction	1
1.1 Aim and Outline of the Thesis	3
2 Literature Review	5
3 Investigated Methods	9
3.1 Resonance Cavity and Microstrip Patch	11
3.2 RGW-Rectangular Waveguide-Microstrip	12
3.3 RGW-Inverted RGW-Microstrip	14
3.4 Back-Short Cavity Method	17
4 Proposed Transitions	21
4.1 Transition for RGW	21
4.1.1 Structure Analysis and Dimensions	24
4.2 Transition for GGW	26
4.2.1 Structure Analysis and Dimensions	26
4.3 Modified GGW Transition for Higher Bandwidth	27
4.3.1 Structure Analysis and Dimensions	29
5 Final Prototypes and Simulated Results	33
5.1 Simulated Results for RGW	33
5.1.1 Coplanar to Microstrip Transition	33
5.1.2 Final Prototype (RGW) and Simulated Results	35
5.2 Simulated Results for GGW	37
5.2.1 Rectangular Waveguide to GGW Transition	37
5.2.2 Final Prototype (GGW) and Simulated Results	38
6 Measured Results	41
6.1 Measurd Results for RGW	41
6.1.1 Manufactured Prototypes and PCB	41
6.1.2 Experimental Setup and Measurements	42
6.2 Measurd Results for GGW	44
6.2.1 Manufactured Prototypes and PCB	44

6.2.2	Experimental Setup and Measurements	45
7	Conclusion and Future Work	49
	Bibliography	51

List of Figures

3.1	Dispersion Diagram for 2D bed of pins. ($h = 1.25mm, g = 0.25mm, w = 0.5mm, d = 1.3mm$)	9
3.2	Dispersion Diagram for a Ridge Gap Waveguide with quasi-TEM mode in the Band Gap. ($a = 1mm, h = 1.25mm, w = 0.5mm, g = 0.25mm, d = 0.8mm, p = 1.3mm$)	10
3.3	Dispersion Diagram for a Groove Gap Waveguide with TE_{10} mode in the Band Gap. ($a = 3.8mm, h = 1.25mm, w = 0.5mm, g = 0.25mm, d = 0.8mm, p = 1.3mm$)	10
3.4	Transition from RGW to Microstrip through Resonance Cavity and Microstrip Patch.	11
3.5	Return loss for resonance cavity-patch transition for different patch width.	11
3.6	Magnitude of E field through the substrate for 60 GHz (left) and 85 GHz (right).	12
3.7	Transition from RGW to Rectangular waveguide to Microstrip- front view (top) and back-view (bottom).	13
3.8	Transition from Ridge Gap Waveguide to Rectangular waveguide.	13
3.9	Transition from Microstrip to Rectangular Waveguide (top lid of back-short is hidden).	14
3.10	Transition from Microstrip to Rectangular Waveguide to RGW- single transition.	14
3.11	Transition from Microstrip to Rectangular Waveguide to RGW- back-to-back transition.	15
3.12	Transition from RGW to Inverted RGW using step transition.	15
3.13	S parameters for transition from RGW to Inverted RGW using step transition.	16
3.14	Design structure for transition from RGW to Microstrip using Inverted RGW.	16
3.15	S parameters for transition from RGW to Microstrip using Inverted RGW.	17
3.16	Step transition from RGW to Rectangular Waveguide.	17
3.17	S parameters for transition from RGW to Rectangular Waveguide.	18
3.18	Design for the back-to-back transition from Microstrip to RGW using backshort cavity.	18
3.19	S parameters for transition from RGW to Microstrip using backshort (single sided).	19

3.20	S parameters for transition from RGW to Microstrip using backshort (back-to-back).	19
4.1	Magnitude of E field at 60 GHz for substrate width - 2 mm (left) and 2.2 mm (right).	21
4.2	Magnitude of E field at 60 GHz for substrate width 1.5 mm with pins at bottom (left) and 2.3 mm with pins om top metal plate (right). . .	22
4.3	Design for the back-to-back transition from Microstrip to RGW using backshort cavity.	23
4.4	S parameters for the back-to-back proposed transition from RGW to Microstrip.	23
4.5	Enlarged version of the transition region with arrows indicating critical dimensions of the structure. ($h_1 = 0.487mm$, $h_2 = 1.013mm$, $h_3 = 1.25mm$, $l_1 = 1.256mm$, $l_2 = 0.916mm$, $l_c = 2.723mm$, $w_c = 0.843mm$, $d_c = 1.188mm$, $w_s = 1.188mm$)	24
4.6	Microstrip Line for RGW with arrows indicating its dimensions. ($Strip_width = 1.5mm$, $Strip_len = 4.42mm$, $w_strip = 0.1mm$, $h_sub = 0.127mm$, $l_marker = 0.1mm$, $extn = 0.42mm$, $len_patch = 1.215mm$)	25
4.7	Design for the back-to-back transition from Microstrip to GGW using backshort.	25
4.8	S parameters for the back-to-back proposed transition from GGW to Microstrip.	26
4.9	Enlarged version of the transition region for GGW with arrows indicating critical dimensions of the structure. ($l_c = 3.751mm$, $w_c = 0.952mm$, $d_c = 1.253mm$, $p_c = 0.65mm$, $p_i = 0.449mm$, $p_o = 0.134mm$)	27
4.10	Microstrip Line for GGW with arrows indicating its dimensions. ($len_sub = 5.52mm$, $width_sub = 1.623mm$, $width_strip = 0.1mm$, $h_sub = 0.127mm$, $marker = 0.1mm$, $exten = 0.422mm$, $len_patch = 1.285mm$)	28
4.11	Design for the back-to-back modified transition from Microstrip to GGW using backshort.	28
4.12	Smith Chart showing S_{11} for the GGW to microstrip transition - without modifying transition region (left) and with modifying transition region (right).	29
4.13	S parameters for the back-to-back modified transition from GGW to Microstrip.	29
4.14	Enlarged version of the modified transition region for GGW with arrows indicating critical dimensions of the structure. ($l_c = 3.389mm$, $w_c = 0.728mm$, $d_c = 0.912mm$, $e_c = 0.387mm$, $e_p = 0.367mm$, $l_b = 1.69mm$, $w_b = 0.239mm$, $h_b = 0.305mm$)	30
4.15	Microstrip Line for modified transition for GGW with arrows indicating its dimensions. ($len_sub = 5.438mm$, $width_sub = 1.52mm$, $w_strip = 0.1mm$, $h_sub = 0.127mm$, $marker = 0.1mm$, $extn = 0.439mm$, $l_patch = 0.977mm$)	30
4.16	S parameters for GGW to Microstrip transition using two discrete ports to terminate the microstrip line.	31

5.1	Back to back transition from co-planar to microstrip line. ($dia_via = 0.24mm$, $gnd_l1 = 0.4mm$, $gnd_l2 = 0.4mm$, $l1 = 0.225mm$, $l2 = 0.175mm$, $l_trans = 0.2mm$, $wstrip1 = 0.05mm$, $wstrip2 = 0.1mm$, $gap = 0.055mm$, $h_sub = 0.127mm$)	34
5.2	S parameters for back to back transition for coplanar to microstrip line.	34
5.3	Port having two modes of excitation for co-planar waveguide- even mode (left), odd mode (right) (HFSS).	35
5.4	Return loss for back to back transition for RGW to Microstrip with PCB modified to comply with manufacturing specification and taking measurements.	35
5.5	Final prototype for the RGW to Microstrip transition. ($len1 = 5.104mm$, $len2 = 18.6mm$, $len3 = 16.852mm$, $len4 = 5.00mm$, $h1 = 2.00mm$, $h2 = 1.50mm$, $h3 = 2.00mm$)	36
5.6	Final PCB Design with Coplanar-Microstrip transition included ($L_s = 4.025mm$, $W_s = 1.47mm$, $l_p = 1.215mm$, $l_e = 0.42mm$, $h_s = 0.127mm$, $w_1 = 0.1mm$, $w_2 = 0.05mm$, $g_p = 0.055mm$, $d_v = 0.24mm$, $d_s = 0.175mm$, $l_n = 0.2mm$).	37
5.7	Simulated S parameters for the final prototype of RGW to microstrip transition for Roger 3010 and Alumina and results verified using HFSS.	37
5.8	Back to back transition from rectangular to GGW. ($width = 1.9mm$, $length = 3.8mm$, $h1 = 0.1mm$, $h2 = 0.1mm$, $len = 1.45mm$)	38
5.9	S parameters for back to back transition for rectangular to GGW.	38
5.10	S parameters for back to back transition for GGW to Microstrip with additional transitions and PCB modified to comply with manufacturing specification and taking measurements.	39
5.11	Final PCB design for GGW to microstrip transition including $25\mu m$ pullback and $30\mu m$ width reduction ($L_s = 5.458mm$, $W_s = 1.49mm$, $h_s = 0.127mm$, $l_e = 0.449mm$, $l_m = 0.1mm$, $w_m = 0.1mm$, $l_p = 0.977mm$)	39
5.12	Final Prototype for GGW to Microstrip Transition ($length = 24.19mm$, $width = 27.6mm$, $height = 21.5mm$, $h1 = 10.0mm$, $h2 = 11.5mm$)	40
5.13	Simulated S parameters for the final prototype of GGW to microstrip transition for Roger 3010 and Alumina and results verified using HFSS.	40
6.1	Manufactured prototype of RGW with PCBs integrated in the transition region.	41
6.2	Manufactured PCB for RGW.	42
6.3	Measurement setup for taking measurement for RGW using GSG probe station.	43
6.4	Measured S parameters for Port 1 and compared to simulated results	44
6.5	Measured S parameters for both the ports of the RGW transition.	44
6.6	Manufactured prototype of GGW with PCBs integrated in the transition region.	45

6.7	Manufactured PCB for GGW.	45
6.8	Measurement setup for taking measurement for GGW using WR-15 Flange.	46
6.9	Measured S parameters for no PCB integrated in the transition region.	47
6.10	Measured S parameters for PCB placed in the transition region through soldering.	47
7.1	RGW Array Antenna with rectangles indicating the possible positions where the MMIC can be integrated.	50
7.2	Conventional method of making transition from MMIC using bondwires which can be replaced with back short cavity transition technique.	50

List of Tables

6.1	Comparison between required and manufactured dimensions for RGW prototype (wrt figure 4.5)	42
6.2	Comparison between required and manufactured dimensions for RGW chip (wrt figure 5.6)	43
6.3	Comparison between required and manufactured dimensions for GW prototype (wrt figure 4.14)	46
6.4	Comparison between required and manufactured dimensions for GW chip (wrt figure 5.11)	46

1

Introduction

Millimeter waves have a wavelength between 10 to 1 mm and covers the frequency spectrum from 30 GHz to 300 GHz. The history of millimeter waves dates back to 1895 when Indian physicist J.C. Bose publicly demonstrated wireless signal links which went high up to even 60 GHz [1]. The first successful wireless signalling experiment by Marconi on Salisbury Plain in England was not until May 1897.

Today the modern society demands high-speed data connectivity, high definition data streaming, radar targeting systems etc. In order to meet such demands there is intense research on a global basis and millimeter wave technologies are leading to a paradigm shift in the communication sector and opening up avenues for new wireless applications. Various industries are expected to develop millimeter wave technologies in the next ten years which are going to have a huge impact in the society. These industries include health care for developing scanning and imaging devices, automotive and transportation for radars and automation, aerospace and defense industry, and telecommunication for making advanced communication devices and high speed data transfer. By the end of this decade it is estimated by analysts that there will be around 50 billion devices like clothes, car, tractors, body sensors etc. which will be connected to each other and also to mobile networks. Such huge network connection demands 1000 times more data and 10 to 100 times more data rate than what today's network can handle. Hence the next generation 5-G systems have to deliver a huge leap in performance to handle mobile network traffic.

However there are various challenges which need to be overcome in order to use millimeter waves in Communication. From the Integrated Circuit Technology point of view there is need for consideration of power consumption, efficiency, dynamic range, linearity requirements etc. At millimeter waves there are three competing IC technologies, namely group III and IV semiconductor technologies such as Gallium Arsenide (GaAs) and Indium Phosphide (InP), Silicon Germanium Technology, and Silicon technology. However no single technology can simultaneously meet all the technical challenges and system requirements. The conventional methods to interconnect PCB circuits are bond wire and flip chips [2, 3, 4, 5]. However these methods have their own limitations. There can be bonding failure due to cratering of a wire-bond pad, wire-bond fracture and lift-off, inconsistent tail etc. Even if a good bond is made there may be reliability failures like intermetallic formation, wire flexure fatigue, wire bond liftoff, electrical noise and so on. These problems associated with bond wires become more severe at millimeter wave frequency due to the small size

of the structure and high frequency. Moreover millimeter wave signals have a high path loss and cannot travel up to very long distance. These waves are non penetrating waves and cannot travel through obstacles like mountains and buildings. In order to have a wide coverage relays or regenerative repeaters are required. The Signal to Noise Ratio (SNR) of the signal is inversely proportional to the square of the frequency, hence at millimeter waves frequency there is a significant reduction in the SNR. The theoretical limit of reliable data transfer rate, Shannon Capacity is given by the equation $C = B * \log_{10}(SNR + 1)$. Hence at millimeter wave frequency the capacity is limited by the low SNR.

The above mentioned problem of bond wire can severely deteriorate the performance of the circuit at millimeter wave, hence new and innovative method needs to be developed. One solution could be is to make contactless interconnection between PCBs through Electromagnetic Coupling [6, 7, 8, 9]. However most work done in Electromagnetic coupling are with direct contact which have its own limitations. A new and innovative idea to make contactless transitions can be done by the use of Gap Waves technology. Gap Waves Technologies had been used earlier for packaging of MMIC Circuits, where getting rid of bond wires and suppression of unwanted modes have been addressed [10, 11, 12]. Using this technique in a smart way it can also be used to make contactless transitions from ridge gap waveguide to Microstrip line, Groove Gap Waveguide to Microstrip line and microstrip to microstrip line by electromagnetic coupling. Such transitions can hence solve various problems of millimeter wave technologies like bondwire, direct contact transitions etc. To deal with low SNR problem at millimeter wave frequencies some techniques like having high gain antennas at transmitter and receivers, and beam steering in order to avoid obstacle have been proposed. [13, 14]. Antenna with high gain can be made using reflector or horn antennas. However, as high gain requires high aperture size these kind of antennas become bulky and not very compatible in terms of installation and portability. Hence array antenna which is planar in shape and is capable of producing pencil beams with high gain is much more attractive solution for communication system. The most typical way to make these array antenna are by microstrip, substrate integrated waveguide (SIW) and rectangular waveguides. Solutions like microstrip and SIW in cheap and low profile but is has losses due to dielectrics and at higher frequencies the losses is significantly high and cannot be used to make high gain array antennas. Rectangular waveguide have very low loss, however fabricating the distribution network for array antenna needs to be done in two metal blocks and then combined. Such techniques at higher frequencies can be problematic as there is possibility of having air gap in between which will degrade the performance drastically. One attractive solution to make array antennas for millimeter and sub millimeter waves is Gap Waveguides [15, 16, 17]. These structures requires an air gap between the metal plates for the waves to travel and hence solves the problem faced by rectangular waveguide. The principal behind the working of this technique is to create Artificial magnetic Conductor (AMC) [18] in the lower metal plate with the help of bed of pins [19] which confines the EM waves on the metal ridge, strip or groove bounded by both sides with high impedance surface. Different kinds of Gap Waveguides can be realised depending upon the required

application. A Ridge Gap Waveguide works supports quasi-TEM mode which is guided through the metal ridge [20]. Groove Gap Waveguide supports quasi TE_{10} mode and is similar to Rectangular Waveguide [21]. There is also inverted microstrip gap waveguide which supports quasi-TEM mode and have a dielectric substrate in between the metal plates [22]. The prototypes of these structures are manufactured by milling or Electronic Discharge Machining (ESD). However these methods are quite expensive and time consuming and not very suitable for mass production and hence there are being investigation done on new and cheap methods to produce these kinds of antennas and one of them being pick and place method.

1.1 Aim and Outline of the Thesis

The above mentioned problems such as high path loss of propagating signals at higher frequencies and interconnects issues between chips due to the extremely small dimensions of chips motivates research in these fields to overcome such issues. The integration of MMIC chip with Gap Waveguide array antenna will not only make the entire system compact but will also reduce the losses in the cables and interconnects of separate antenna and circuit System. Integration of power amplifiers and phase shifters to the feed network of gap waveguide array antenna can help to deal with the problem of high propagation loss through beam steering to avoid obstacle. For millimeter wave the dimensions of the waveguides and interconnects in the structure becomes very small and hence contact transition from MMIC to waveguides or MMIC to MMIC is not a feasible option. Moreover, direct contact with the MMIC can lead to internal fracture, create unwanted noise and provides less flexibility, hence these transitions needs to be contactless.

Contactless transition from Microstrip to Ridge Gap waveguide and Microstrip to Groove Gap Waveguide have been presented in this thesis. These transitions are suitable for integration of RF MMIC with the feed network of gap waveguide array antennas. These transitions are compact and also provides an easy solution for the packaging of the MMIC chips. The method proposed here can also be used to make transition from Microstrip to Microstrip thus replacing the traditional method of bond wire and flip chip to connect RF circuits. However, this part is not covered in the thesis.

Chapter 2 contains the works which have been done earlier regarding transitions from microstrip to rectangular waveguide and microstrip to ridge gap waveguide. Chapter 3 presents the investigated methods which could be used for making a transition from Microstrip to Gap Waveguides. A brief discussion about each of the proposed transition is presented in this chapter. Chapter 4 contains the final proposed microstrip to gap waveguide transition. Both the ridge gap waveguide and groove gap waveguide transitions had been optimised and the final results have been presented and discussed. Chapter 5 contains the final prototypes for the ridge gap waveguide and groove gap waveguide transitions which had been manufactured. Coplanar to microstrip line transition and rectangular waveguide to microstrip transitions are also presented here which had been included for measurement purpose.

In Chapter 6 the measured results for both Ridge and Groove Gap Waveguide transitions are presented and compared to the simulated results. Finally in Chapter 7 conclusion is presented based on the simulated and measured results and the future work which can be done based on the work done based in this thesis.

2

Literature Review

As explained earlier in the previous chapter, Gap Waveguide technology can provide an attractive solution to deal with the problems of high frequency signals. Some initial papers verifying this gap waveguide concept have been cited [15, 16, 17, 18, 19, 23, 24]. In this Chapter we discuss about the various works on transitions especially from microstrip to rectangular waveguide and some papers on transitions from microstrip to ridge gap waveguide which had been done earlier.

Transitions from chip to chip had been done earlier through electromagnetic coupling [6, 7, 8, 9], however these transition require a direct contact between them. The most common and popular way to make a transition from microstrip to rectangular waveguide is through a probe combined with backshort. In University of Massachusetts Yoke-Choy Leong designed probe transition for microstrip substrate with various dielectric constants ranging from 2.2 to 13 in two orientation relative to the waveguide (broadside and longitudinal) [25]. The experimental verification for the two orientation of the design had been done for the W-Band. The GARD group working in the ALMA project and the Microwave group in Microtechnology and Nanoscience of Chalmers work a lot with transitions from Microstrip to Rectangular waveguide using probe backshort method. A waveguide to Microstrip transition with an integrated bias-T had been designed for X-band device which had a return loss better than -20 dB, insertion loss of about -0.15 dB and had a RF bandwidth for the transition of about 30% for the central frequency [26]. Kunio Sakakibara of Nagoya Institute of Technology had developed a transition using two backshort one by short-circuited waveguide and the other by the microstrip substrate its self. With such backshort and using extended ground for tuning a bandwidth of about 32.5% had been achieved [27].

However all these kinds of backshort are in the broadside or longitudinal direction relative to the waveguide. For integration purpose it is more convenient if the microstrip is inside the waveguide itself, in the plane of the rectangular waveguide walls. Transitions where the microstrip is in the same plane as that of the waveguide walls have been done earlier using step transitions from Rectangular waveguide to Microstrip. A wide band, low insertion loss transition from Microstrip to rectangular Waveguide had been designed for 17-22 GHz [28] and for V-Band [29]. However these transitions are quite complex in terms of architecture and hard to manufacture. Moreover these kind of transitions normally requires a direct contact with the microstrip. Contactless transition from microstrip to Rectangular waveguide have also been reported using Yagi antenna to radiate out the electromagnetic waves into

the waveguide [30]. The microstrip was integrated in the E-Plane for X-band with alumina substrate. It had a 35% bandwidth with a return loss better than -12 dB and insertion loss of about -0.3 dB. However the design of the yagi antenna occupies a lot of space in the PCB and more over it have a complex design architecture hence not very suitable for MMIC integration.

Work related to transition from microstrip to Ridge Gap waveguide through pressure contact had been done earlier [31]. The transition is based on the fact that both ridge gap waveguide and microstrip have similar filed distribution (quasi TEM mode). Hence it is possible to make a matching from the quasi TEM mode of air (Ridge gap waveguide) to quasi TEM mode in substrate (Microstrip). A standard Chebychev transformer based on several quarter wavelength sections of different width can be employed to make the transition. However in this paper to make it suitable for integration with MMIC only one step transition was used. The chosen length of the ridge gap waveguide was about 42 mm, which was around four times the wavelength at 30 GHz. The back-to-back simulated result showed return loss below -15 dB over a bandwidth of about 55%. The measured return loss was below -14.5 dB over the bandwidth of 23-43 GHz and had an insertion loss better than 0.32 dB. However this kind of transition need a direct contact between the ridge and the Microstrip which will not only lead to loading effect but could also damage the MMIC. As frequency increases it will become more difficult to make a good direct contact between the ridge and the MMIC due to the decrease in the dimensions. Moreover this transition requires the substrate thickness to be same as that of the air gap of the ridge gap waveguide hence making it less flexible.

Work on contactless transition from Microstrip to ridge gap waveguide has also been done earlier by electromagnetic coupling [32, 33]. The working principal included overlapping of a quarter wavelength of the ridge with the patch of the microstrip line. The ridge had a length of 11.6 mm (approximately 4λ) and two additional side ridge section that overlapped the patch of the PCB. After optimization it was found that the width of the path and the matching part of the ridge had similar dimensions and the gap between the substrate and the and the ridge was $63 \mu m$. An additional pin was also added just after the transition in order to get rid of unwanted modes that may start propagating. The simulated result for F band showed a return loss larger than 15 dB with a relative bandwidth of 23.6% and the insertion loss was lower than 1.3 dB over this bandwidth. However the tolerance level of this transition was very low. The PCB was manufactured by ATC which had a tolerance of $\pm 2.54 \mu m$ for the conductor and gap dimensions, $\pm 51.0 \mu m$ for hole diameter and hole location and $\pm 25.4 \mu m$ for overall PCB dimension. With such tolerance level the measured result showed a return loss only below 5 dB. A study in order to see the tolerance level of such transition was also done using Monte Carlo Simulation. Parameters like gap misalignment between the top PCB and the bottom of the pins at each port, PCB horizontal mismatch and PCB rotational mismatch was taken into account in the simulation to find out the most sensitive parameters. The study showed that if a good transition below 15 dB return loss is needed for this structure with a reliability of 90% the maximum tolerance in the gap between the substrate

and the ridge can be $\pm 10\mu m$. Hence this structure is really very sensitive to the height of the gap between the ridge and the substrate. It is quite challenging to manufacture structures with an accuracy below $\pm 10\mu m$ and use of high precision equipment are expensive and requires lots of time for its manufacture. So such sensitive structure is not suitable for mass production.

Hence there was need to investigate new methods to make transitions from microstrip to Gap waveguide which will be reliable and more robust for integration of MMIC chips with Gap waveguide antennas. In the following Chapters we discuss the investigated methods to make such transitions followed by the proposed transition, the final prototypes with simulated and measured results.

2. Literature Review

3

Investigated Methods

An investigation was initially done about the various works on transitions which had been done so far. Contact transitions through electromagnetic coupling [6, 7, 8, 9], transitions using backshort methods [25, 26, 27], transitions from rectangular waveguide to microstrip with microstrip in the plane of the waveguide wall [28, 29, 30] and also some works done for transition from ridge gap waveguide to microstrip [31, 32, 33]. In this chapter some investigated methods which seemed to be promising to make transition for Ridge Gap Waveguide (RGW) to Microstrip is presented. The proposed idea and motivation behind each transition, and reason why a particular transition didn't work will also be discussed briefly. The investigation was done to make transition from Ridge Gap waveguide to Microstrip and the final proposed method to make the transition was also implemented for Groove Gap Waveguide. Three investigated methods to make RGW to microstrip transition (Resonance Cavity and Microstrip Patch, RGW to Rectangular waveguide to Microstrip, RGW to Inverted RGW to Microstrip) along with the final proposed transition using backshort cavity have been discussed in the sections below.

In order to have a gap waveguide first the dimension of the pins, the distance between the pins and the gap between the pins and the top metal plate need to be defined using a trial and error method to have a band gap for the required frequency band. Such dimensions should be defined taking into consideration the manufacturing feasibility. Guide lines regarding dimensions of pin and pin spacing have been

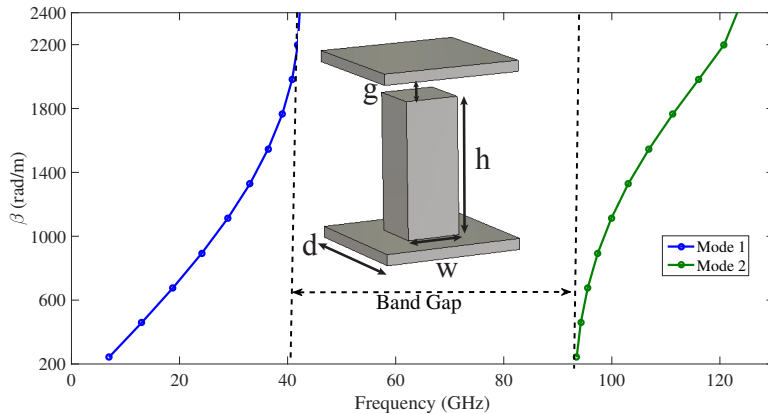


Figure 3.1: Dispersion Diagram for 2D bed of pins. ($h = 1.25mm$, $g = 0.25mm$, $w = 0.5mm$, $d = 1.3mm$)

3. Investigated Methods

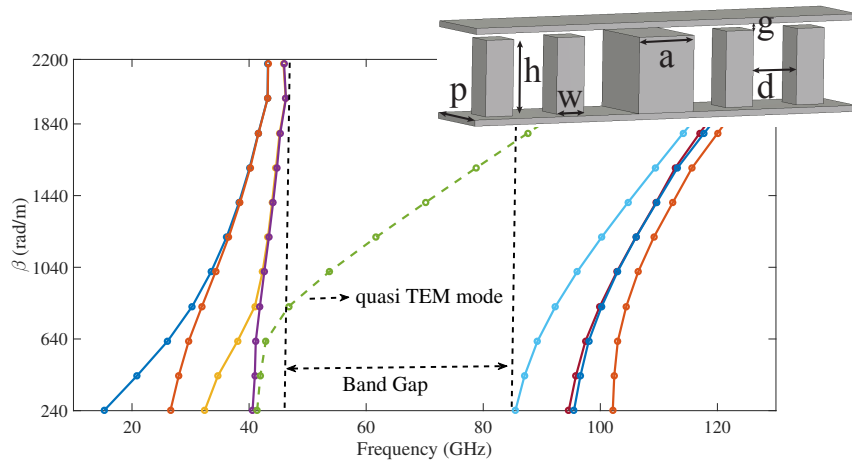


Figure 3.2: Dispersion Diagram for a Ridge Gap Waveguide with quasi-TEM mode in the Band Gap. ($a = 1\text{mm}$, $h = 1.25\text{mm}$, $w = 0.5\text{mm}$, $g = 0.25\text{mm}$, $d = 0.8\text{mm}$, $p = 1.3\text{mm}$)

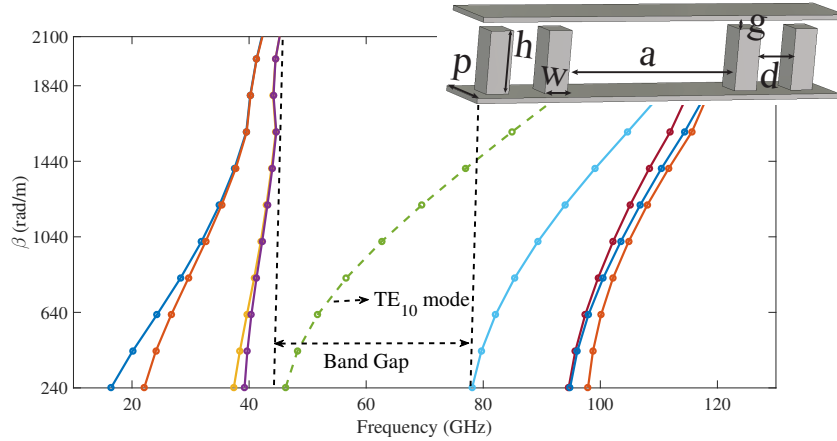


Figure 3.3: Dispersion Diagram for a Groove Gap Waveguide with TE_{10} mode in the Band Gap. ($a = 3.8\text{mm}$, $h = 1.25\text{mm}$, $w = 0.5\text{mm}$, $g = 0.25\text{mm}$, $d = 0.8\text{mm}$, $p = 1.3\text{mm}$)

given in [19]. Figure 3.1 shows the band gap diagram of a 2-D layer pins along with the pins structure. As seen in the figure two modes can travel through the bed of pins and there is a band gap from 42 GHz to 90 GHz. This means waves which lies in the frequency range of 42-90 GHz cannot pass through the bed of nails. If some perturbation to the periodic bed of pins structure is introduced having the correct shape and dimension it is possible to propagate a mode within the band gap. Such perturbation can be a ridge or a groove introduced to the periodic structure of bed of pins. The waves lying within the band gap cannot travel through the pins and it remains confined to the ridge or groove.

Figure 3.2 shows the Dispersion diagram for Ridge Gap Waveguide. As seen from the figure the band gap exist from 45-85 GHz and within the band gap quasi-TEM mode propagate through the ridge. Figure 3.3 shows the Dispersion Diagram for a Groove Gap Waveguide. It have similar band gap as that of the Ridge Gap Waveguide with TE_{10} mode propagating through the groove. It is necessary to have

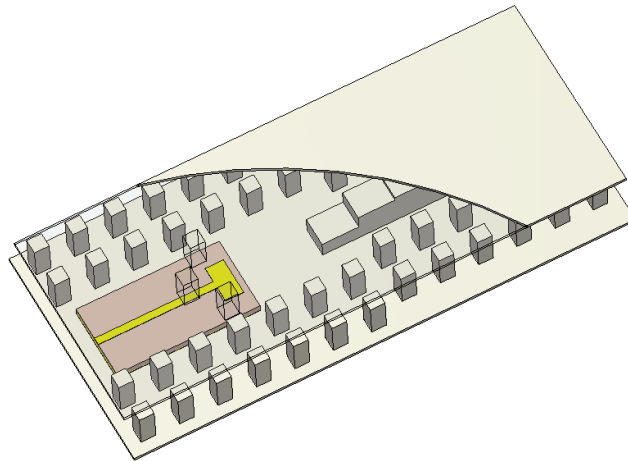


Figure 3.4: Transition from RGW to Microstrip through Resonance Cavity and Microstrip Patch.

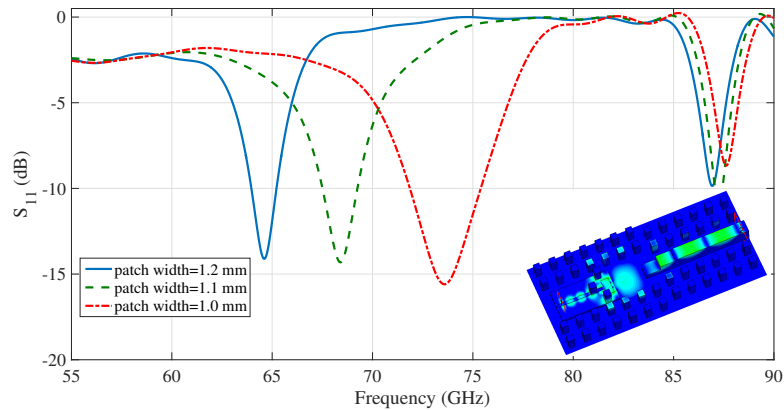


Figure 3.5: Return loss for resonance cavity-patch transition for different patch width.

a standard dimensions of pins and ridge which will provided the necessary band gap before investigating any transitions. Below the dispersion diagrams the proposed dimensions of the pins, ridge and the groove have been given for which contactless transition had been investigated and finally fabricated.

3.1 Resonance Cavity and Microstrip Patch

The figure 3.4 shows the proposed design idea for making transition from RGW to Microstrip using Resonance Cavity and microstrip patch. Here the top metal plate is hidden to show the structure of the proposed transition. A transition from RGW to GGW can be done through impedance matching by using a step from RGW to GGW. The waves in the GGW can then be used to make a resonance cavity by applying pins to the top metal plate at a distance of about $\lambda/2$ from the ridge. These pins also is used to suppress any unwanted modes in the microstrip after the

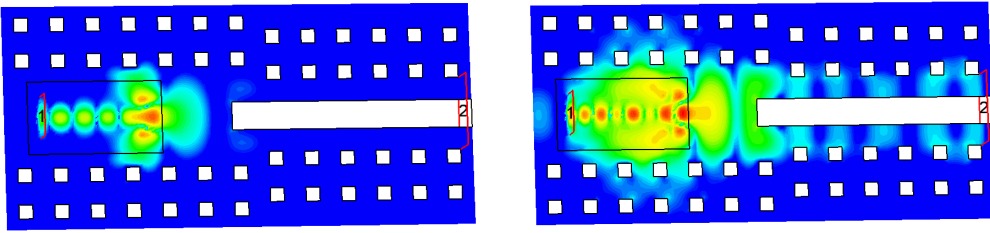


Figure 3.6: Magnitude of E field through the substrate for 60 GHz (left) and 85 GHz (right).

waves have coupled from the resonance cavity to the microstrip.

It is a well known fact that patch used as a radiator have a very narrow bandwidth and the required frequency range which needs to be covered is from 57-66 GHz (V-Band) which is about 15% bandwidth with respect to 60 GHz. However, a patch couples radiation from all its edges and depending on the length and width of the patch there should be two resonance frequencies. The idea was to tune the length and width of the patch and bring the two resonance frequency close to each other so that the overall bandwidth could cover from 57-66 GHz. Figure 3.5 shows the reflection coefficient (S11) for the transition. It can be seen from the plot that there are two dips for each for the curve which was speculated to be the two resonance frequencies.

However it was noticed that with the change in the dimensions (length and width) of the patch the resonance frequency around 60 GHz changed and the one around 85 GHz remained constant. In order to make a proper investigation the magnitude to E field was observed in various layers of the structure both for 60 and 85 GHz. As seen in figure 3.6 for 60 GHz we have a resonance in the patch (red elliptical region) and then the waves propagate through the strip with quasi TEM mode. However, for 85 GHz no resonance was observed and waves also propagate through the substrate. Hence, it was concluded that the dip in the reflection coefficient at 85 GHz was due to leakage through the substrate and not due to resonance. It was finally concluded that coupling through microstrip patch from a resonance cavity is very narrow band and cannot be used for MMIC integration.

3.2 RGW-Rectangular Waveguide-Microstrip

There are several transitions which have been done earlier from microstrip to rectangular waveguide. One of such transition using backshort have been done in Nagoya Institute of Technology, Japan [27]. Transition from rectangular waveguide to RGW using probe are used from designing RGW Array antennas [23, 24]. One way to make a transition from Microstrip to RGW is to combine these two techniques. Figure 3.7 shows the back-to-back transition for the proposed design. In this designed the transition have been done for E band (60-90 GHz) with Microstrip substrate as Teflon which have an $\epsilon_r = 2.1$. However similar design using higher permittivity of the substrate for V Band can also be designed and it is estimated that there may be a slight reduction in bandwidth due to high permittivity of substrate.

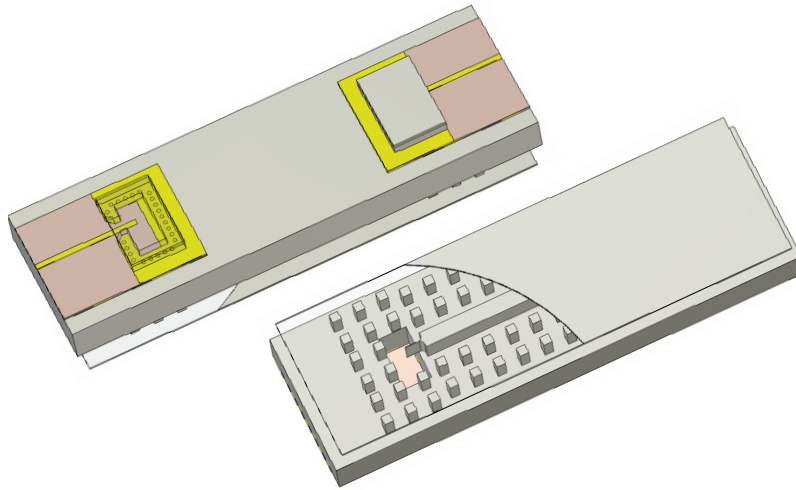


Figure 3.7: Transition from RGW to Rectangular waveguide to Microstrip- front view (top) and back-view (bottom).

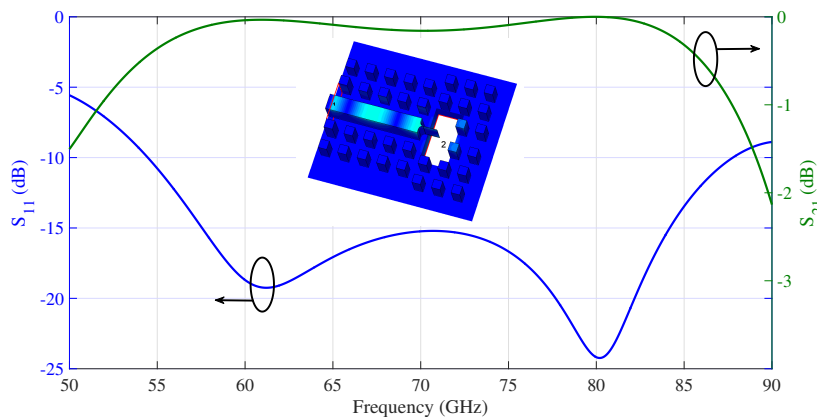


Figure 3.8: Transition from Ridge Gap Waveguide to Rectangular waveguide.

The transition from RGW to Rectangular waveguide is done with a probe in order to match the impedance if the RWG to the Rectangular waveguide. Figure 3.8 shows the S Parameters of the transition and it can be seen from the plot that the return loss better than 10 dB have a bandwidth of 45%. Figure 3.9 shows the simulated transition from Microstrip to Rectangular Waveguide using back-short which have a relative bandwidth of 37% for return loss better than 10 dB. However, using this kind of backshort it not very convenient for integrating MMIC chips. Other replacement for this back-short are planar transition in multi-layer substrate and planar transition in single layer substrate [27]. However these planar transitions are not very wide band especially the single layer and investigation needs to be done to make transition using these planar layers. Here in order to verify that such transition from microstrip to RGW can be done we have used the back-short method. Figure 3.10 and 3.11 show the simulated results for single and back-to-back transition respectively and it have a bandwidth of 31% for a return loss better than 15 dB. However, this transition is not very suitable for integrating MMIC with

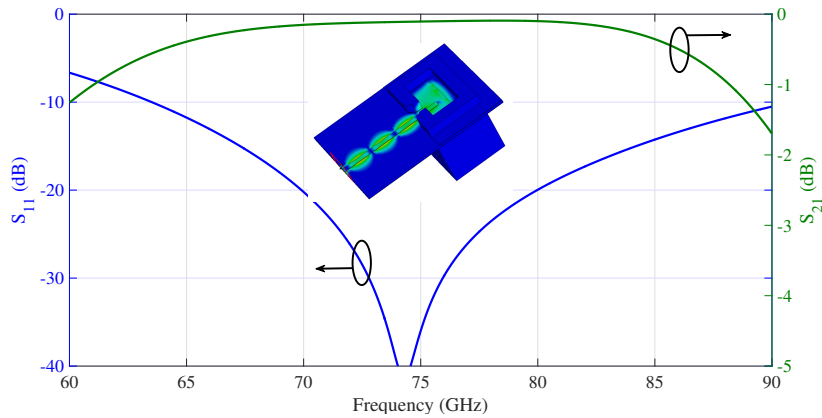


Figure 3.9: Transition from Microstrip to Rectangular Waveguide (top lid of backshort is hidden).

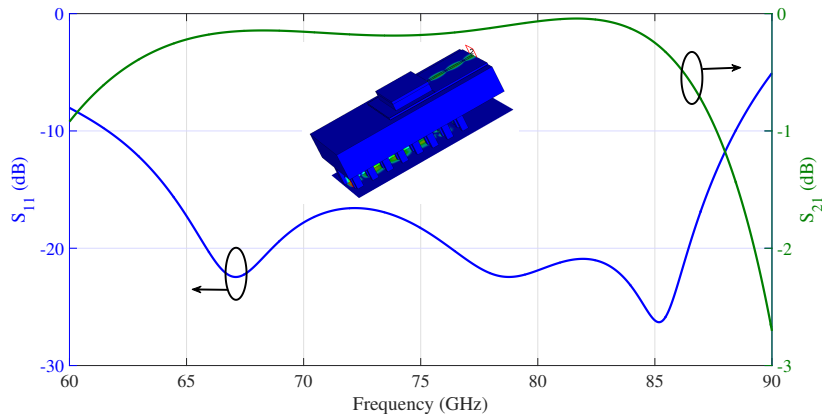


Figure 3.10: Transition from Microstrip to Rectangular Waveguide to RGW- single transition.

Gap waveguide antenna as we need an external backshort to make this transition. Moreover, the microstrip is in the plane opposite of the plane of the pins, which is not appropriate as many of the RGW array antenna have its radiating plane where the microstrip have been integrated. The most appropriate place to integrate the MMIC chip is in the plane of the pins as then it gives the freedom to have radiating slots of the array antenna on either side of the RGW. Moreover, for the mass production of such RGW array antenna with integrated MMIC "pick and place" method could be a suitable option. In this case having the MMIC in the plane of the pins will be most convenient for using this method. Hence, more investigation was done to make a transition from RGW to Microstrip where the microstrip is in the plane of the pins.

3.3 RGW-Inverted RGW-Microstrip

The earlier works on transition between RGW to Microstrip have been done with the microstrip on the top metal plate above the ridge [31, 32, 33]. The reason is the

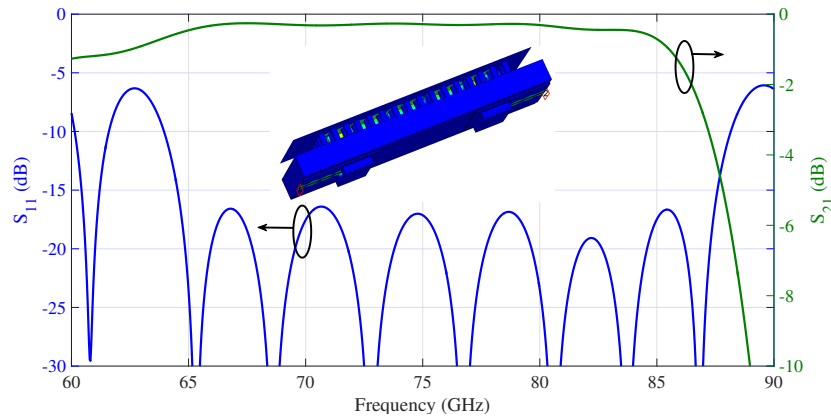


Figure 3.11: Transition from Microstrip to Rectangular Waveguide to RGW- back-to-back transition.

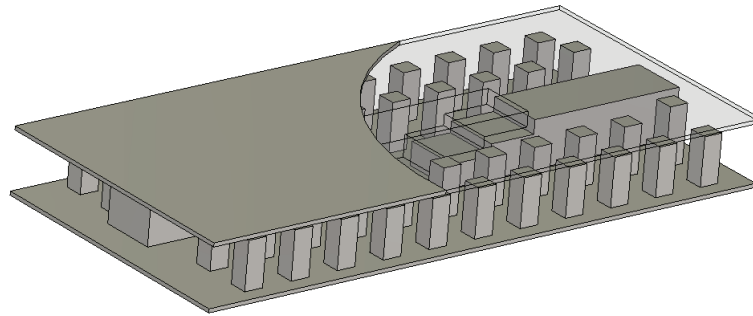


Figure 3.12: Transition from RGW to Inverted RGW using step transition.

ease to couple the waves from the RGW to Microstrip as in both these structures the waves travel as quasi TEM mode. As a result of this the impedance matching between the two structures becomes simpler and also gives a wide bandwidth.

However, with the microstrip in the plane of the pins it becomes more difficult to match the impedance between them. The idea of this transition was to make a transition in order to transfer the quasi TEM mode travelling in the ridge to quasi TEM mode on the plane of the pins. In order to do this a concept of Inverted Ridge Gap Waveguide have been introduced where the ridge is on the top metal plate and the air gap for the waves to travel is in the plane of the pins. Transition from RGW to Inverted RGW can be done using a step transition. Figure 3.12 shows the designed transition from ridge to inverted Ridge Gap Waveguide using steps for impedance matching. The gap in between the steps is about 0.22 mm which is close to the gap between the ridge and the metal plate (0.25 mm). Such a transition is really very wide band and covers the entire frequency band which the RGW can support (45-90 GHz). The S parameters for this transition is shown in figure 3.13. As seen from the plot this transition have a very good return loss of about -20 dB for a large section of the frequency band.

Using such step transition to Inverted RGW, transition can be done to Microstrip through electromagnetic coupling. Figure 3.14 shows the designed transition for

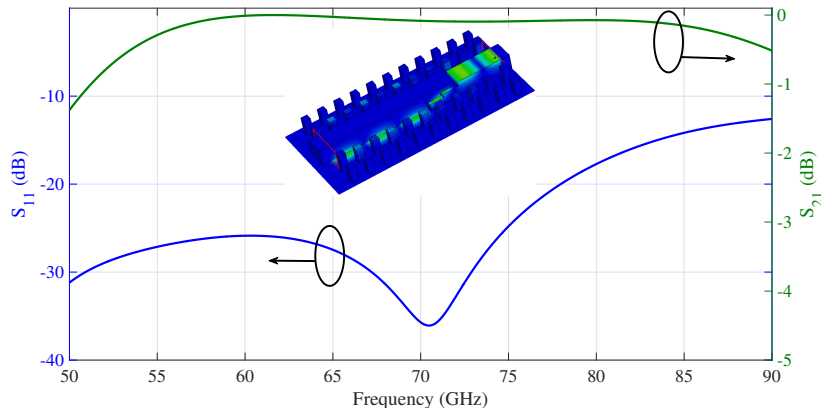


Figure 3.13: S parameters for transition from RGW to Inverted RGW using step transition.

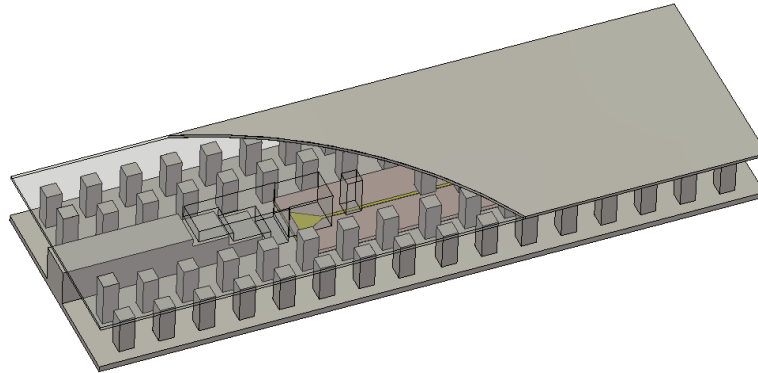


Figure 3.14: Design structure for transition from RGW to Microstrip using Inverted RGW.

the Microstrip in the plane of the pins. The material used in the simulation for the microstrip is Roger 3010 with an $\epsilon_r = 10.2$. The reason for using such high permittivity substrate is we want to integrate the MMIC chips which have a high relative permittivity above 10. Here in this design radial patch have been used instead of the regular rectangular patch. The top metal plate contains two additional pins just after the transition in order to suppress any unwanted modes which may be there in the microstrip after the transition. The length of the overlapping impedance matching ridge just after the steps on the top metal plate is about 1.4 mm which is close to $\lambda/4$ wavelength. The width of the overlapping matching ridge is similar to the width of the ridge (1.19 mm). The length of the patch overlapping the ridge is also around $\lambda/4$ and the width of the patch is same as that of the ridge. The gap between the matching ridge and the substrate is 0.124 mm.

Figure 3.15 shows the S parameters for the designed transition. As seen from the plot the return loss of the structure is better than 15 dB for the entire frequency band of (55-71 GHz). A return loss better than 10 dB have a bandwidth of around 30%. The bandwidth achieved in the previous work was about 24% [33] and hence, it shows that radial patch gives a better bandwidth performance as compared to

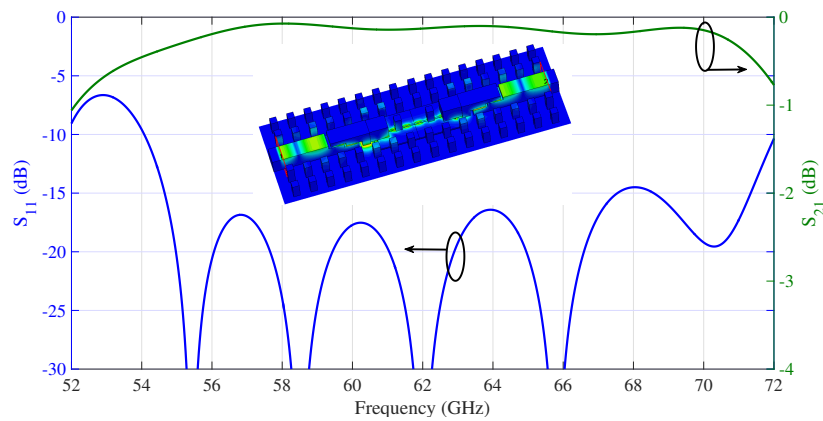


Figure 3.15: S parameters for transition from RGW to Microstrip using Inverted RGW.

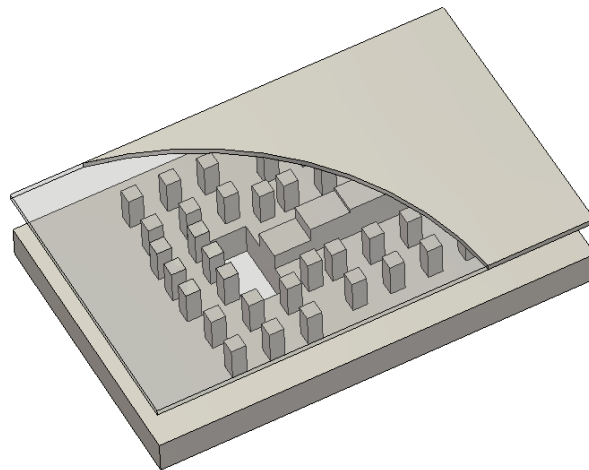


Figure 3.16: Step transition from RGW to Rectangular Waveguide.

rectangular patch. However, as mentioned earlier these kind of contactless transition is very sensitive to the air gap between the ridge and the microstrip and requires precision below $10\mu m$. It is not feasible to produce structure with this high accuracy. Hence, new robust method to make transition from Gap waveguide to Microstrip was needed.

3.4 Back-Short Cavity Method

Making a robust transition which will be contactless is a challenging task. Back-short methods to make transitions from waveguides are pretty reliable and robust with minor problems of higher order modes due to leakage [25, 26, 27]. Moreover, for backshort method the microstrip is not in the plane of the walls of the Rectangular waveguide. Hence, this is not a suitable method for integration of MMIC chips with gap waveguide array antennas. Therefore, more innovative backshort needed to be invented in order to come up with a solution for integrating MMIC with gap

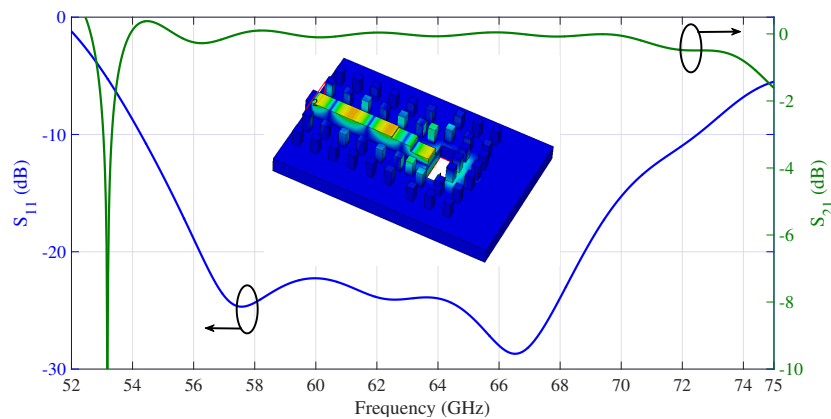


Figure 3.17: S parameters for transition from RGW to Rectangular Waveguide.

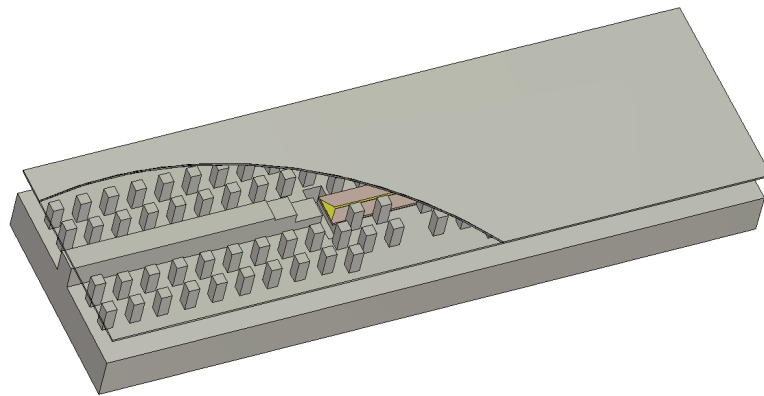


Figure 3.18: Design for the back-to-back transition from Microstrip to RGW using backshort cavity.

waveguide array antennas.

Transition from RGW to rectangular waveguide using a probe had been done earlier as shown in figure 3.8. The idea was to make a transition from RGW to rectangular waveguide. A backshort can then be applied to this rectangular waveguide to form a cavity. Waves can be coupled from this cavity to microstrip line by placing a probe above the cavity. The gap wave pins can be positioned around the cavity in a smart way for impedance matching. These pins can also be used to suppress any unwanted modes that may be present and hence avoid leakage. However, as seen in figure 3.8 the E plane probe from the ridge cover the major portion of the rectangular waveguide which prohibits the placing of the microstrip probe above the rectangular cavity. In order to place the probe above the rectangular cavity the transition from ridge to the rectangular waveguide should be such that no portion of the ridge is extending into the rectangular waveguide. In order to make such a transition a step structure from the ridge to the rectangular waveguide have been proposed.

Figure 3.16 shows the proposed step transition from RGW to rectangular waveguide. And figure 3.17 shows the S parameters of the proposed transition. As seen from the plot this transition have a return loss better than 10 dB over 30% bandwidth and

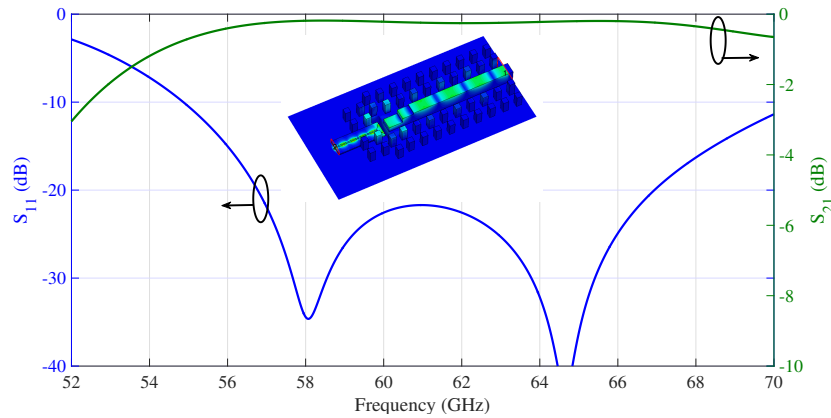


Figure 3.19: S parameters for transition from RGW to Microstrip using backshort (single sided).

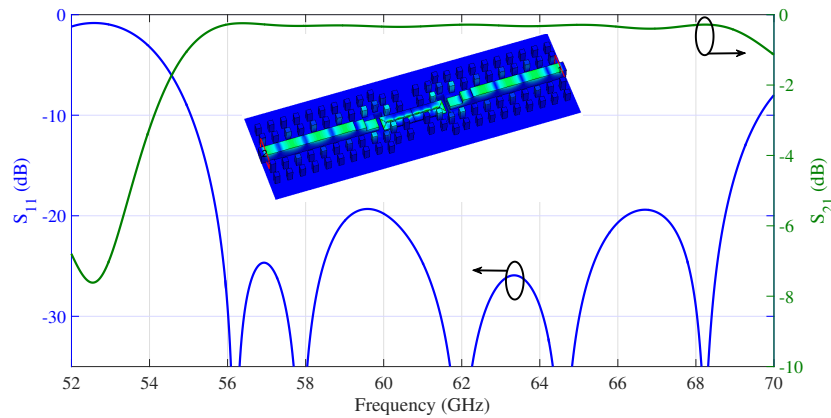


Figure 3.20: S parameters for transition from RGW to Microstrip using backshort (back-to-back).

the performance of this transition is same as that of the E plane probe transition for V Band. This transition is more appropriate from the manufacturing point to view as there is no taper protruding into the waveguide. This step transition from RGW to rectangular waveguide had been used from making microstrip-RGW transition. Finally applying a $\lambda/4$ back-short and placing a radial probe above the rectangular cavity the waves was coupled from the cavity to the microstrip. In the simulation Roger 3010 with an $\epsilon_r = 10.2$ was used which is close of the relative permittivity of MMIC substrate. Figure 3.18 shows the back-to-back structure of the designed transition. In this figure the top metal plate is hidden in order to get a view of the actual structure. The pins around the back-short and the microstrip was adjusted so that there is no leakage or higher order modes present. Figure 3.19 shows the one sided S parameters for the transition. As seen from the plot it has a return loss better than 15 dB over 20% bandwidth and return loss better than 10 dB over 23% bandwidth. The S parameters for back-to-back transition as shown in figure 3.20 gives similar results with a return loss around 20 dB for almost the entire band of frequency (56-69 GHz).

3. Investigated Methods

In the following chapter a detail discussion for the backshort cavity method is given. Dimensions of the designed transition, various orientations in which the pins can be placed and effect on impedance due to the microstrip with high ϵ_r is discussed. RGW-microstrip transition has been presented using the backshort cavity method. This backshort cavity method has then been implemented for GGW-microstrip transition. GGW-microstrip transition had also been modified in order to achieve higher bandwidth.

4

Proposed Transitions

As mentioned earlier that transition using backshort are pretty stable and are widely used to make transition in RF circuits. However, in these transitions the Microstrip is not in the plane of the waveguide walls and hence integrating a chip inside the waveguide array antenna using backshort is not possible using the typical architecture. In this chapter we discuss about the method using $\lambda/4$ cavity and gap wave technology introduced in section 3.4. RGW-microstrip transition is initially presented. This backshort cavity method is then presented for GGW-microstrip transition. Some smart modification near the transition region in order to increase the operating frequency band for the GGW-microstrip transition had also been done.

4.1 Transition for RGW

Transition from RGW to microstrip can be done by step transition to have impedance matching between RGW and rectangular waveguide. A $\lambda/4$ backshort to form a rectangular cavity can then be made and the signal can be transferred to microstrip using radial probe through EM coupling. The position of the pins near the transition region is important. If in the transition region the pins are in the plane of the ridge then the microstrip have a limitation on the maximum width which it can have. This is due to the fact that if the width is more than $\lambda/2$ then modes can travel into the cavity as TE modes of GGW instead of travelling as quasi TEM mode through the microstrip.

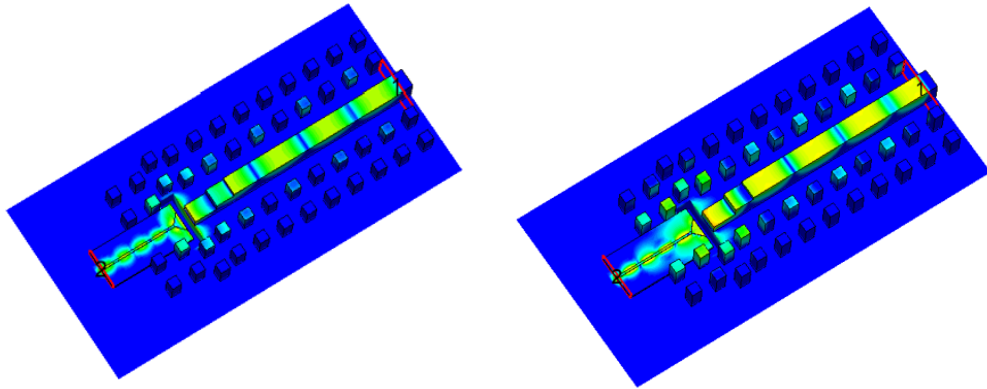


Figure 4.1: Magnitude of E field at 60 GHz for substrate width - 2 mm (left) and 2.2 mm (right).

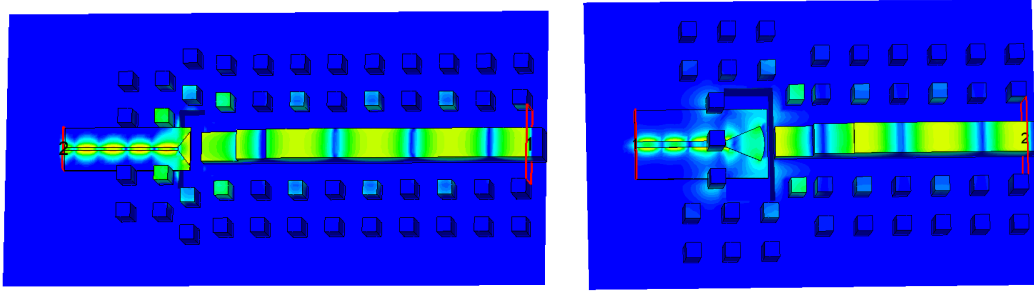


Figure 4.2: Magnitude of E field at 60 GHz for substrate width 1.5 mm with pins at bottom (left) and 2.3 mm with pins on top metal plate (right).

Figure 4.1 shows the transition which is optimised for microstrip width of 1.5 mm and thereafter the width was increased to investigate at what width there is leakage due to unwanted modes in the cavity. As seen from the figure at 2 mm there is no leakage and only quasi TEM modes travel through the microstrip. With further increase in microstrip width (2.2 mm) leakage starts as the width is around $\lambda/2$ for 60 GHz. Hence, it was concluded for pins in the plane of the ridge the maximum width which microstrip can have so that there is no leakage is 2mm. However, if the width needs to be more than 2 mm, transition can be done by placing the pins on the top metal plate near the transition region. Transitions with pins on the top metal plate have also been investigated and the results are similar to the one with pins at the bottom. One interesting observation for pins at the top plate was that the size of the rectangular cavity was increasing with the increase in the width of the microstrip after optimization. The reason for this is the high permittivity of the substrate placed above the cavity ($\epsilon_r = 10.2$) which affects the impedance of the rectangular cavity. In order to compensate for the increase in impedance of the cavity, the cavity becomes larger as the impedance decreases with the increase in the width of the rectangular waveguide.

Figure 4.2 shows two transitions with microstrip width as 1.5 mm and 2.3 mm. As seen from the figure the microstrip with 2.3 mm width after optimization covers the entire rectangular cavity thus increasing the impedance of the transition region. In order to compensate this increase the optimized cavity dimension becomes larger. As seen in figure 4.2 the size of the cavity after optimization is much larger for microstrip with 2.3 mm width as compared to microstrip with 2mm width. Smart design techniques can be used to handle this problem. Some possible solutions which can be investigated is to cover the entire width of the cavity with the substrate and optimize to have the minimum possible cavity size and use elliptical cavity. For the proposed transition substrate width of 1.5 mm had been used and the extension of the substrate into the cavity had been reduced so that the cavity could be as small as possible.

Figure 4.3 shows the proposed back-to-back transition from Microstrip to RGW. As seen in this structure the transition has microstrip on either side of the back-to-back transition which is different from the actual scenario for integration in which the ridge will be in either side as shown in figure 3.18. This is done from the measurement point of view as it is not possible to take measurement using a convenient method

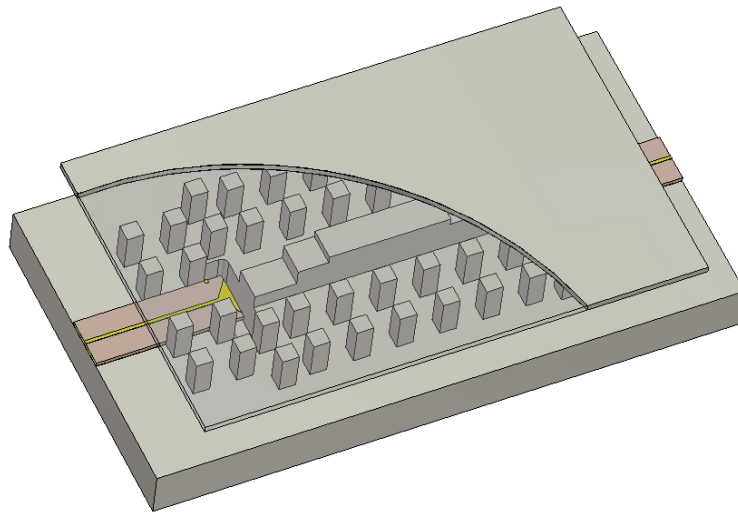


Figure 4.3: Design for the back-to-back transition from Microstrip to RGW using backshort cavity.

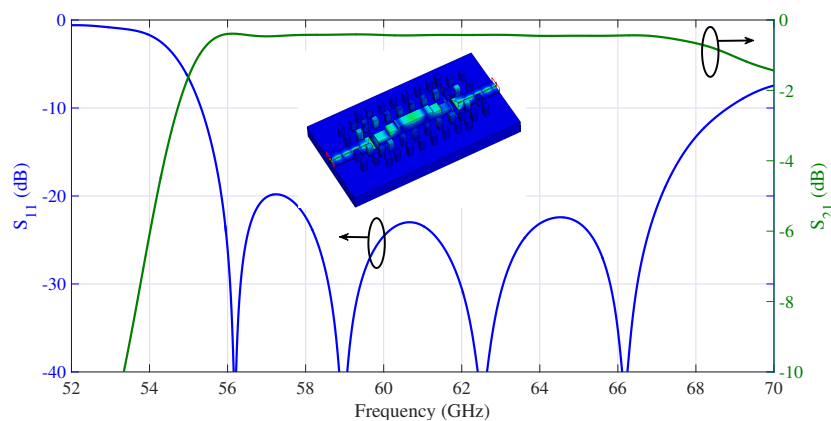


Figure 4.4: S parameters for the back-to-back proposed transition from RGW to Microstrip.

to excite the ridge. The microstrip on the other hand can be excited by making a transition from coplanar to microstrip and using a Ground Signal Ground (GSG) probe. Therefore it was necessary to make a Microstrip-RGW-Microstrip transition.

Figure 4.4 shows the S parameters of the transition from Microstrip to RGW. As seen from the figure the transition have return loss better than 20 dB over 18.3% and better than 10 dB over 21.14%. This is slightly smaller than the bandwidth achieved with the back-to-back case with microstrip in the middle as shown in figure 3.20. The reason for this is that both these transitions had been optimised separately and the length of the structures are also different, hence constructive and destructive interference of waves occur in different frequencies for these two structures leading to the slight change in bandwidth.

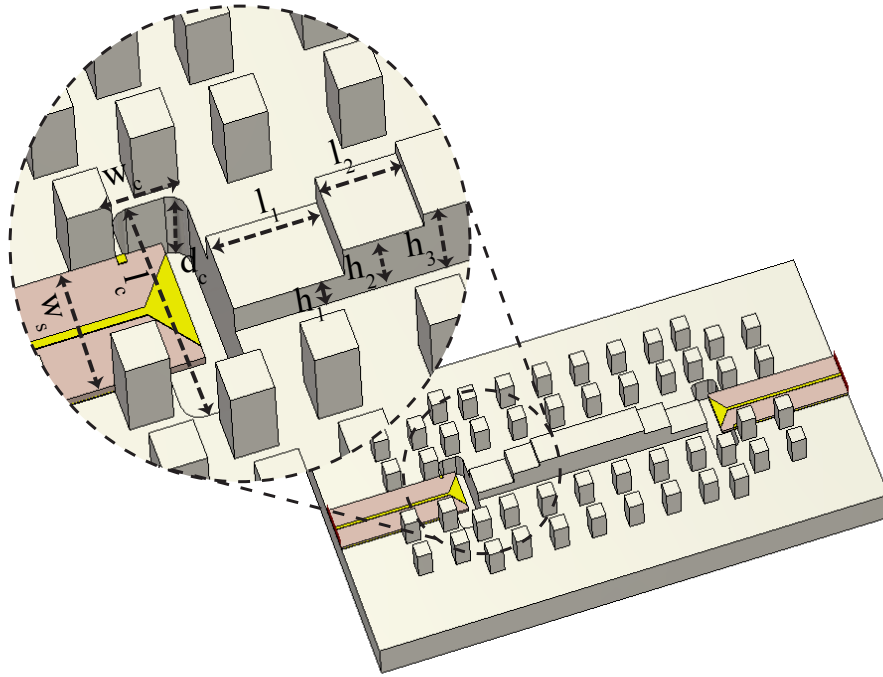


Figure 4.5: Enlarged version of the transition region with arrows indicating critical dimensions of the structure. ($h_1 = 0.487mm$, $h_2 = 1.013mm$, $h_3 = 1.25mm$, $l_1 = 1.256mm$, $l_2 = 0.916mm$, $l_c = 2.723mm$, $w_c = 0.843mm$, $d_c = 1.188mm$, $w_s = 1.188mm$)

4.1.1 Structure Analysis and Dimensions

Figure 4.5 shows the transition region for Microstrip to RGW along with arrows indicating the dimensions which needs to be optimised to get a good impedance matching. The cavity size used for backshort theoretically should have a length of $\lambda/2$ and depth of $\lambda/4$. The impedance of the TE mode of a rectangular waveguide is given by $Z_{TE} = \frac{k\eta}{\beta}$ where $\beta = \sqrt{k^2 - k_c^2}$ and $k_c = \sqrt{(m\pi/a)^2 + (n\pi/a)^2}$. Using these formulas we can calculate the impedance of the TE_{10} mode to be around 505Ω . It is also to be noted that the impedance of the backshort region will slightly be altered due to the high ϵ substrate. On the other hand the impedance of the RGW can be calculated by approximating the RGW with a microstrip having substrate thickness as the air gap between the ridge and the top metal plate (0.25 mm) and the width of the microstrip as the width of the ridge (1 mm). Using predefined impedance formula or by using analytical line impedance in CST it is found that the impedance of the RGW is about 50Ω . Hence we need to match the 50Ω of the RGW to the 505Ω of the backshort. Such impedance matching can be done using Chebyshevs matching transform each of $\lambda/4$ where the impedance of the RGW is increased by decreasing the height of the ridge. Here as seen in figure 4.5 we have used a two quarter wave transform for the impedance matching. However the number of steps can be increased to have a better matching but in that case the structure will become more elongated which may not be suitable for MMIC integration. Figure 4.5 shows the dimensions of the RGW after optimization of

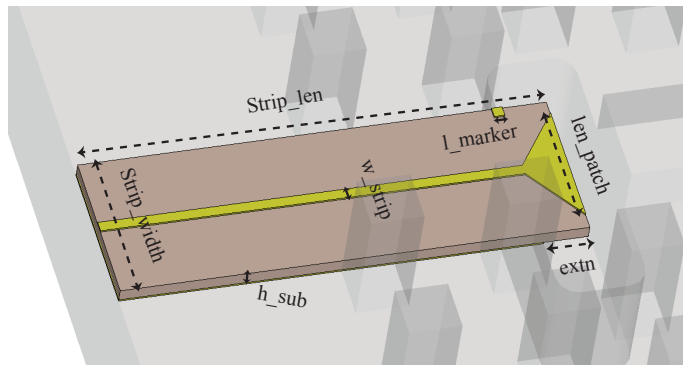


Figure 4.6: Microstrip Line for RGW with arrows indicating its dimensions. ($Strip_width = 1.5mm$, $Strip_len = 4.42mm$, $w_strip = 0.1mm$, $h_sub = 0.127mm$, $l_marker = 0.1mm$, $extn = 0.42mm$, $len_patch = 1.215mm$)

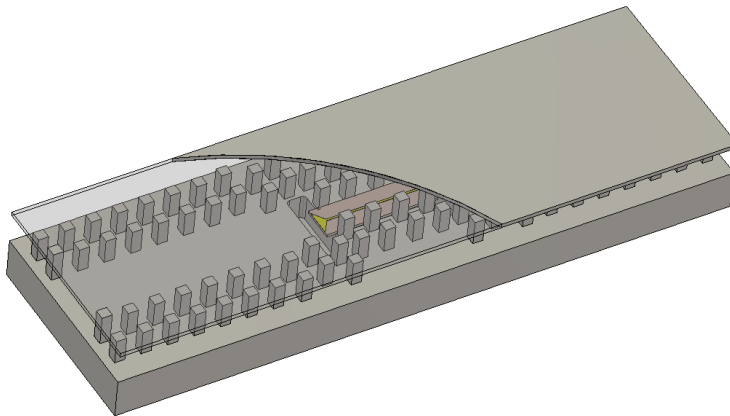


Figure 4.7: Design for the back-to-back transition from Microstrip to GGW using backshort.

the return loss. These dimensions corresponds to the S parameters for the back-to-back transition in figure 4.4. As seen in the figure the optimised value is in line with the theoretically predicted results, the length of cavity = $\lambda/2 \sim l_c = 2.723$, length of matching section = $\lambda/4 \sim l_1 = 1.256 \sim l_2 = 0.916$ and depth of cavity = $\lambda/4 \sim d_c = 1.188$.

Figure 4.6 shows the designed microstrip with radial patch and arrows indicating the various dimensions of the PCB. The optimised dimensions corresponds to the S parameters in figure 4.4. The substrate used here is Roger 3010 with an $\epsilon_r = 10.2$ and height of the substrate is 0.127 mm. The corresponding 50 Ω transmission line has a microstrip width (w_strip) of 0.1 mm. The length of the substrate extended into the backshort ($extn$) is 0.42 mm which is about half of the width of the backshort. It can also be seen in figure 4.6 there is a small square patch of 0.1 mm dimension which is used as a marker to accurately position the PCB on the RGW.

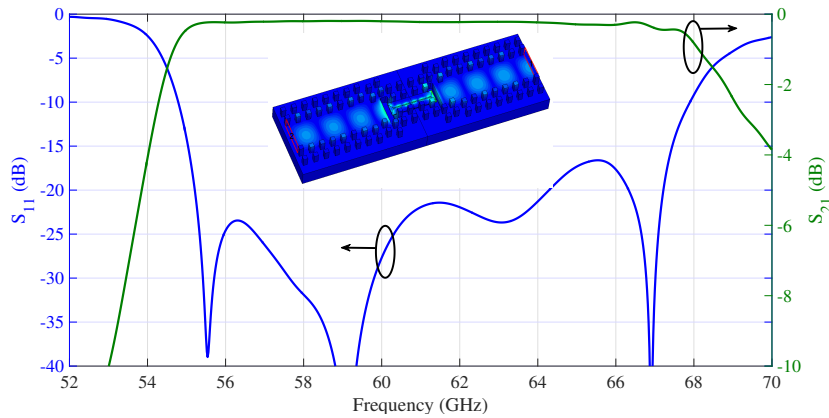


Figure 4.8: S parameters for the back-to-back proposed transition from GGW to Microstrip.

4.2 Transition for GGW

As stated earlier that the method proposed to make transition between microstrip to RGW can also be extended to transition from microstrip to GGW. Figure 4.7 shows the proposed transition for the GGW. As seen from the figure it has similar architecture as that of the RGW transition. The S parameters of the transition are shown in figure 4.8. As seen from the plot the insertion loss is better than 0.5 dB and the return loss is better than 20 dB for almost the entire band from 55-68 GHz. The bandwidth of this transition is 21.14% which is similar to the RGW transition. Here too the substrate used is Roger 3010 with $\epsilon_r = 10.2$. However like in the case of the RGW impedance matching is not possible by changing the height of the ridge. In this case the position of the first two pins just after the backshort had been changed in order to have an impedance matching from the groove to the microstrip. Similar to the step transition in RGW we can change the positions of more number of pins, however changing the positions of two pins were enough to get a good result.

4.2.1 Structure Analysis and Dimensions

Figure 4.9 shows the transition region for GGW to Microstrip transition and the arrows indicate the critical dimensions of the structure for transition. The dimensions after optimization are given below the figure and correspond to the S parameters in figure 4.8. The dimension of the cavity is similar to the one in RGW with $d_c = \lambda/4 \sim 1.253\text{mm}$. However $l_c = 3.751\text{mm} > \lambda/2$. This is because the groove is made 0.38 mm wide to match it with WR-15 ($3.8\text{mm} \times 1.9\text{mm}$) waveguide flange, standard waveguide used for V Band (frequency range of 50-75 GHz). Hence the cavity has to have similar dimensions to have an impedance matching from GGW to microstrip. In figure 4.9 it can be noticed that the first set of pins just after the backshort had moved inside the groove making the groove smaller unlike the second set of pins which had moved outside making the groove larger. This is similar to gap wave filter or diplexer design [34] where the position, shape and size of the pins is used to pass certain frequencies through the structure. Here the first pin after

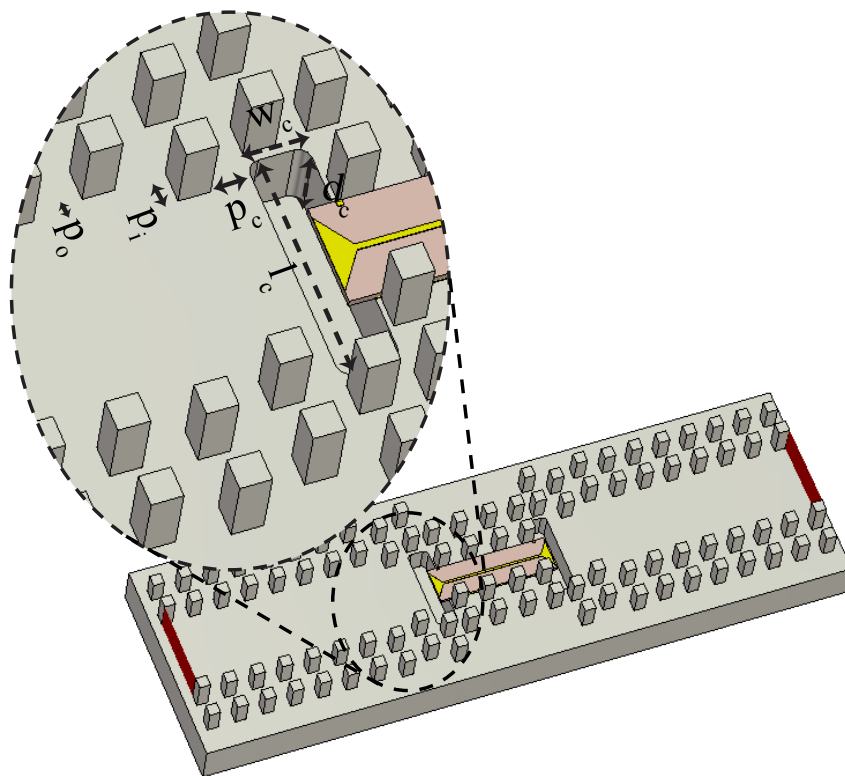


Figure 4.9: Enlarged version of the transition region for GGW with arrows indicating critical dimensions of the structure. ($l_c = 3.751mm$, $w_c = 0.952mm$, $d_c = 1.253mm$, $p_c = 0.65mm$, $p_i = 0.449mm$, $p_o = 0.134mm$)

the backshort is at a distance ($p_c + w_c/2 = 0.65 + 0.952/2 = 1.126mm$) $\sim \lambda/4$ from the transition region. The first pair of pins after the backshort is extending into the groove has reflection from the pins and there is reflection also in the transition region. As these two reflection are $\lambda/4$ apart they interfere destructively and the return loss is minimized. Figure 4.10 shows the structure of the microstrip along with its optimised dimensions which corresponds to the S parameters in figure 4.8. As it can be seen from the dimensions given below the figure that the optimised values dimensions for the microstrip for both the RGW and GGW transitions are similar.

4.3 Modified GGW Transition for Higher Bandwidth

Figure 4.11 shows the structure of the RGW with modified transition for higher bandwidth. Here in this transition the pins of the groove have been aligned in a straight line, and instead of changing the position of the pins for matching the first pair of pins after the backshort have been elongated. The reason is to have the same effect of destructive interference of waves to minimize the return loss which had been discussed earlier. Moreover such elongated pins acts as inductive iris which is used to have matching in the transition region. There is also a small block just

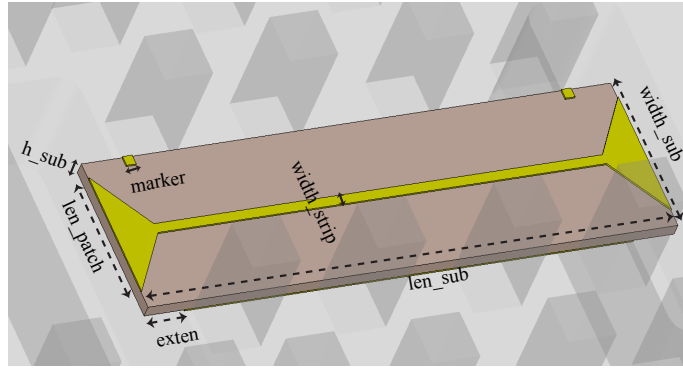


Figure 4.10: Microstrip Line for GGW with arrows indicating its dimensions. ($len_sub = 5.52mm$, $width_sub = 1.623mm$, $width_strip = 0.1mm$, $h_sub = 0.127mm$, $marker = 0.1mm$, $exten = 0.422mm$, $len_patch = 1.285mm$)

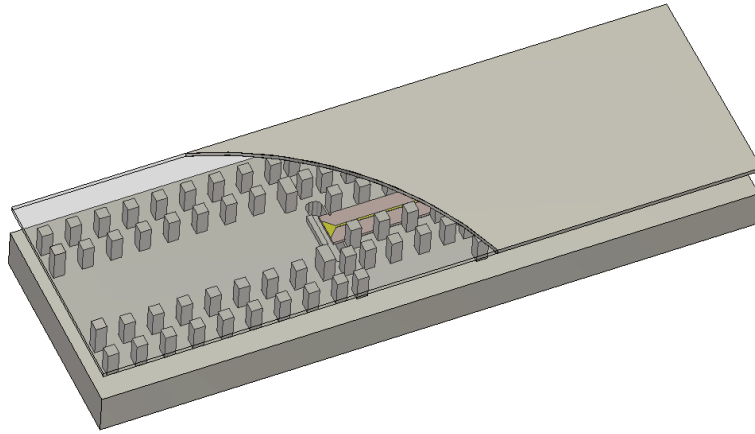


Figure 4.11: Design for the back-to-back modified transition from Microstrip to GGW using backshort.

after the backshort cavity as seen in the figure which actually acts as a capacitive iris [35] to tune out the inductance in the circuit to give a matching over a larger frequency range. In order to have a better understanding of how more bandwidth is achieved using capacitive iris we analyse the Smith Chart in 4.12. In the figure the left Smith chart is of the GGW to microstrip transition without any modification in the transition region and corresponds to the S parameters in figure 4.8. As it can be seen from the smith chart the more we go towards higher frequency beyond 68 GHz (S_{11} below -10 dB till 68 GHz) the S_{11} becomes more inductive. Hence if a good matching at higher frequencies is need these inductance need to be canceled out using capacitive iris. It is to be noted here by using such capacitive iris there is need to optimise the entire transition region again which will lead to the change in the dimensions of the structure.

The right smith chart in figure 4.13 shows the S_{11} of the transition from GGW to microstrip using capacitive iris after optimization. The corresponding S parameters in dB is shown in figure 4.13. As it can be seen from the figure the return loss better than 10 dB is covered from 54 GHz to 71 GHz which is about 27.2% bandwidth

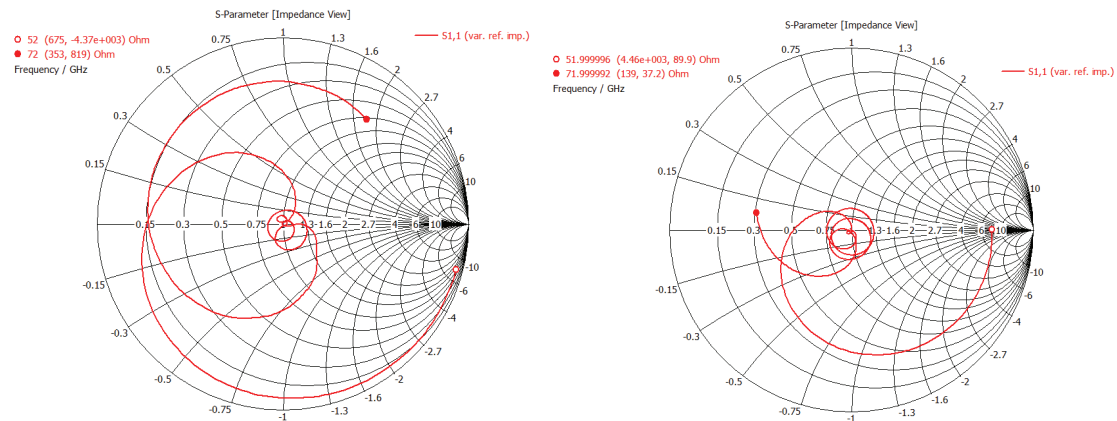


Figure 4.12: Smith Chart showing S_{11} for the GGW to microstrip transition - without modifying transition region (left) and with modifying transition region (right).

as compared to 21.14% bandwidth which had been achieved earlier. It is also to be noted that the matching was better for transition without capacitive iris ($S_{11} \sim -20dB$) as compared to the transition with capacitive iris ($S_{11} \sim -15dB$). Hence it can be concluded that the initial transition gave a better matching and the modified transition gave better bandwidth as seen in figures 4.8 and 4.13

4.3.1 Structure Analysis and Dimensions

Figure 4.14 shows the enlarged version of the modified transition region for GGW to microstrip transition. The dimensions after optimisation is given below the figure 4.14 and corresponds to the S parameters in figure 4.13. As it can be seen from the

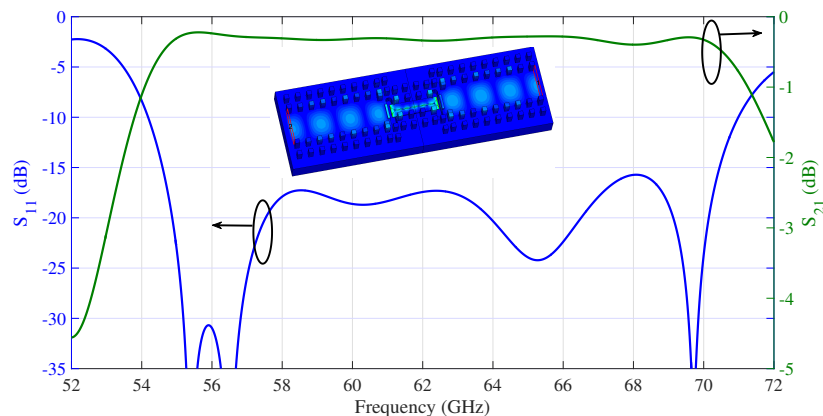


Figure 4.13: S parameters for the back-to-back modified transition from GGW to Microstrip.

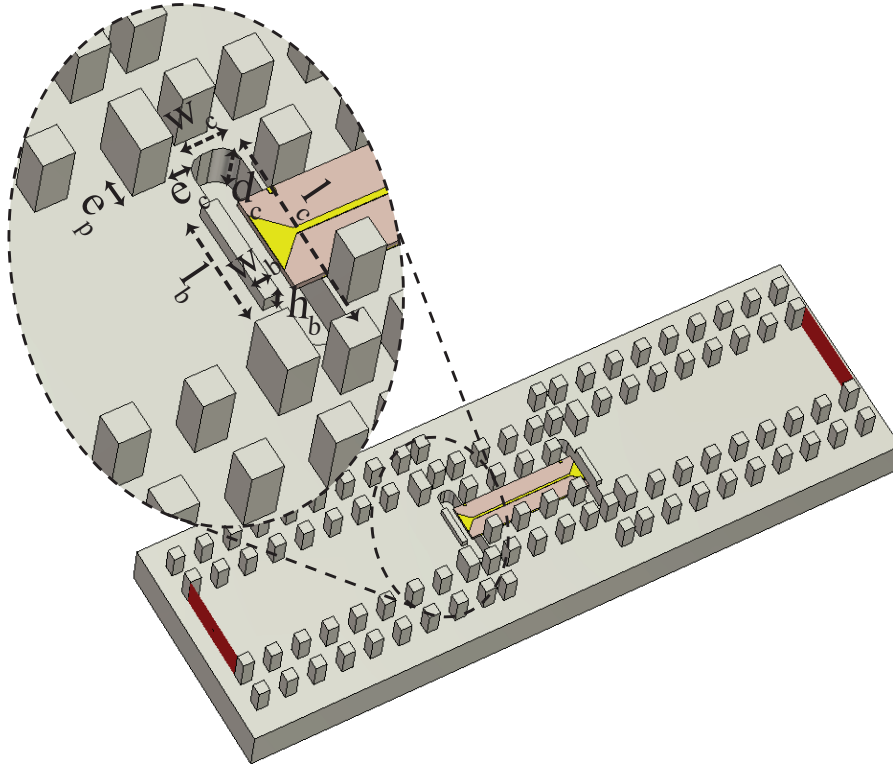


Figure 4.14: Enlarged version of the modified transition region for GGW with arrows indicating critical dimensions of the structure. ($l_c = 3.389mm$, $w_c = 0.728mm$, $d_c = 0.912mm$, $e_c = 0.387mm$, $e_p = 0.367mm$, $l_b = 1.69mm$, $w_b = 0.239mm$, $h_b = 0.305mm$)

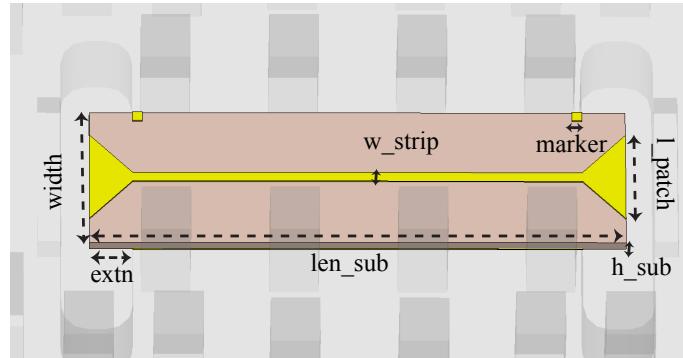


Figure 4.15: Microstrip Line for modified transition for GGW with arrows indicating its dimensions. ($len_sub = 5.438mm$, $width_sub = 1.52mm$, $w_strip = 0.1mm$, $h_sub = 0.127mm$, $marker = 0.1mm$, $extn = 0.439mm$, $l_patch = 0.977mm$)

figure there is a reduction in the dimensions of the backshort cavity as compared to the previous transition without capacitive iris. This is advantageous from the MMIC integration point of view as it will make the structure more compact. Unlike the previous case the distance of the first pair of pins after the backshort is ($e_c + w_c/2 = 0.751mm$) less than $\lambda/4$. However taking into account the surface of the block which

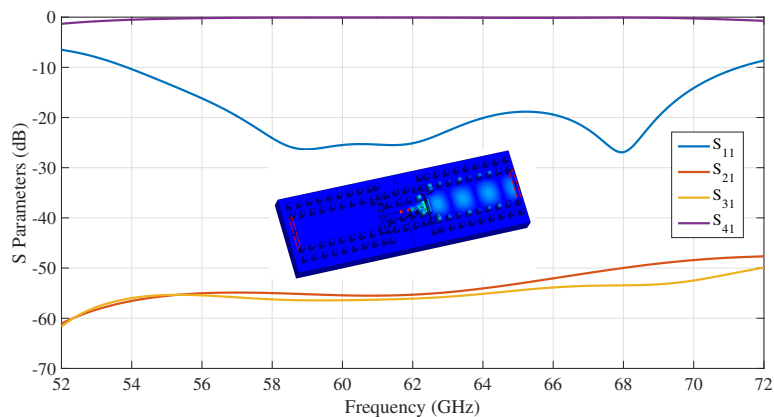


Figure 4.16: S parameters for GGW to Microstrip transition using two discrete ports to terminate the microstrip line.

is placed just after the backshort the total length the waves needs to travel after the first pair of pins is approximately $\lambda/4$ ($e_c + w_c/2 + 2 * h_b = 1.361mm$). Figure 4.15 shows the proposed microstrip design with radial probe along with its dimensions for the optimised structure.

As a final check to verify that this kind of cavity method used as backshort to make a transition actually works and the S parameters received are not due to leakage or some other kind of abnormalities, two discrete port in the microstrip line is introduced along with the previous two waveguide ports. Such discrete port is set to 50Ω in order to match with the impedance of the microstrip line. The waveguide port is excited and the corresponding microstrip line just after the transition is terminated using 50Ω discrete port 4. As seen in figure 4.16 the S_{11} is below -20 dB which shows that there is good impedance matching in the transition region, S_{41} is above -0.5 dB which proves that the microstrip line have 50Ω impedance and the signal propagates through the microstrip line and S_{31} and S_{21} is below -50 dB which shows that there is no coupling of signals to these ports. Hence we can finally conclude that the received S parameters for this kind of transition is due to good impedance matching and signal propagating through the microstrip and not due to leakage of any sort.

4. Proposed Transitions

5

Final Prototypes and Simulated Results

The final aim of the project was to manufacture the proposed transitions for RGW and GGW and compare the measured results with the simulated results. In this chapter the final proposed prototypes for the RGW and the GGW is presented. These prototypes includes the final packaging of the RGW and GGW transitions presented in the previous chapter so that it could be fabricated and experimental measurements can be done on it. CPW to Microstrip transition and Rectangular Waveguide (WR-15) to GGW transition is also discussed which are added to the previously optimised RGW and GGW transitions. Some changes in the PCB had also been done to take into account the manufacturing tolerance. The changes in S parameters due to additional transition and PCB modification have also been presented below.

5.1 Simulated Results for RGW

Microstrip can be excited by making a transition from coplanar waveguide (CPW) to microstrip line and using Ground Signal Ground probe. In this section we discuss about back to back transition between co-planar to microstrip line and the proposed dimensions for such transition. The effect on S parameters for the proposed RGW to microstrip transition when this additional CPW-microstrip transition is added is also discussed.

5.1.1 Coplanar to Microstrip Transition

There are several things which needed to be considered for making the coplanar to microstrip transition. The GSG probe which is used to take measurements had a pitch (distance between signal and ground) of $100\ \mu m$ and hence the dimensions of the coplanar waveguide needed to be set accordingly. These PCBs are manufactured using photo-lithography process and the gap and lines have a tolerance level of $\pm 2.54\ \mu m$ and the diameter and holes location have a tolerance level of $\pm 51\ \mu m$. The minimum dimension of line and gap which can be achieved is $\pm 25.4\ \mu m$. Taking all these into consideration the transition from coplanar to microstrip had been designed. Figure 5.1 shows the proposed back to back transition from coplanar to microstrip line along with its dimensions.

Figure 5.2 corresponds to the S parameters of the back to back transition proposed

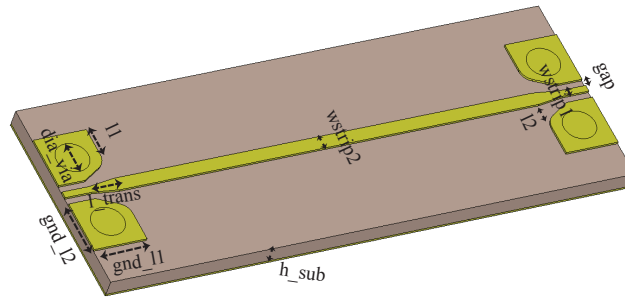


Figure 5.1: Back to back transition from co-planar to microstrip line. ($dia_via = 0.24mm$, $gnd_l1 = 0.4mm$, $gnd_l2 = 0.4mm$, $l1 = 0.225mm$, $l2 = 0.175mm$, $l_trans = 0.2mm$, $wstrip1 = 0.05mm$, $wstrip2 = 0.1mm$, $gap = 0.055mm$, $h_sub = 0.127mm$)

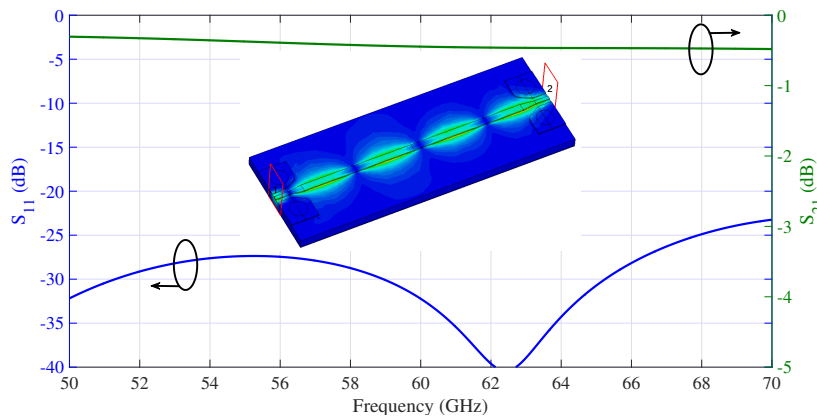


Figure 5.2: S parameters for back to back transition for coplanar to microstrip line.

in figure 5.1. As it can be seen from the figure the transition have a return loss better than 20 dB and a insertion loss better than 0.5 dB over the entire range of frequencies (50-70 GHz). Here it is worth mentioning that there is no well defined method to define a waveguide port for coplanar waveguide. In the simulations done here for coplanar waveguide Frequency Domain Solver in CST had been used which was found to be relatively easier to use and giving results similar to predicted results. It is also to be noted that the coplanar waveguide supports odd and even modes which can propagate through it as shown in figure 5.3. Figure 5.2 shows the S parameters for the even mode which have a good matching from coplanar to microstrip line and almost all the odd mode is reflected back (S_{11} below -50 dB). This had been verified using HFSS simulation. However from measurement point of view GSG probes are widely used to transfer signals from coplanar to microstrip and hence it is definite that even modes propagate through the probe.

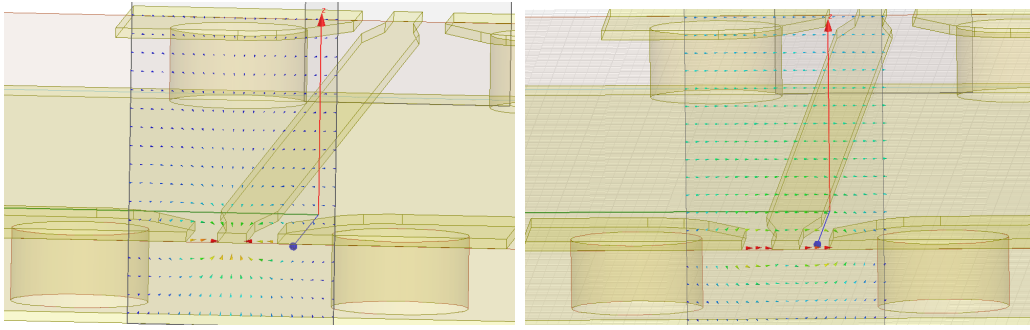


Figure 5.3: Port having two modes of excitation for co-planar waveguide- even mode (left), odd mode (right) (HFSS).

5.1.2 Final Prototype (RGW) and Simulated Results

The above mentioned back to back coplanar to microstrip transition had been included to the optimised RGW to microstrip transition. Figure 5.4 shows the transition without coplanar waveguide (same as figure 4.4) and also the transition with coplanar waveguide. As seen from the two plots including the coplanar waveguide effect the entire transition to a negligible extent and the return loss (S_{11}) is better than 15 dB. From the manufacturing point of view there are other changes in the PCB which needs to be included. There is need to add a minimum $25 \mu m$ 'pullback' (gap between the edge of the PCB and copper layout) to protect the layout while splicing the PCB board. The entire dimension of the PCB have a tolerance level of $\pm 25.4 \mu m$ and the milling process also have tolerance level of few microns. Hence if the dimensions of the PCB and the space to place the PCB are same, due to tolerance there may be dimension mismatch and the PCB may not fit in the prototype. To take this into account an addition reduction of $15 \mu m$ in the width on each side had been included to the previous transition with coplanar waveguide. The last plot in figure 5.4 shows the S parameters of the transition after including 'pullback' of $25 \mu m$ and gap of $15 \mu m$ to the previous transition with CPW. The simulation results shows that there is not much change in the return loss due to such changes which

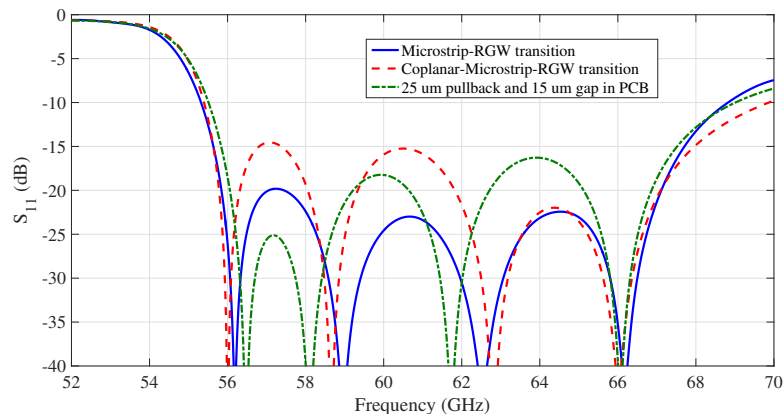


Figure 5.4: Return loss for back to back transition for RGW to Microstrip with PCB modified to comply with manufacturing specification and taking measurements.

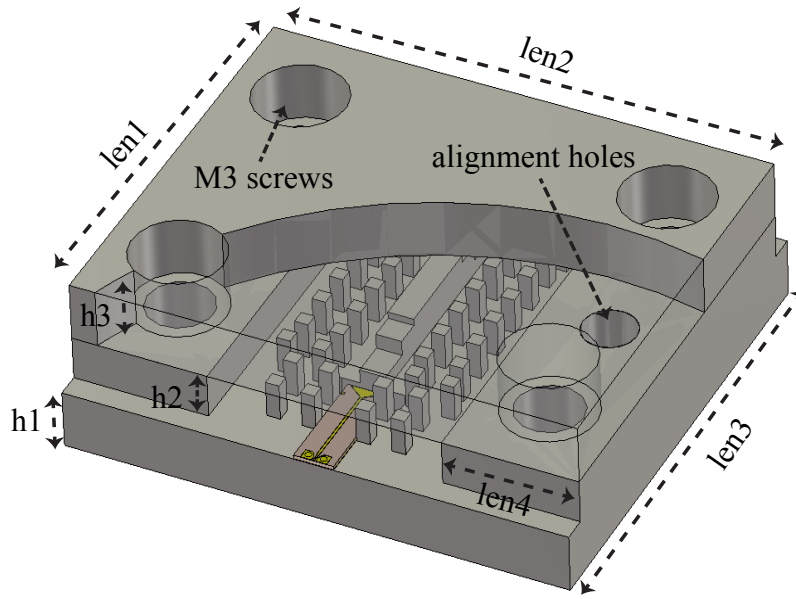


Figure 5.5: Final prototype for the RGW to Microstrip transition. ($len1 = 5.104mm$, $len2 = 18.6mm$, $len3 = 16.852mm$, $len4 = 5.00mm$, $h1 = 2.00mm$, $h2 = 1.50mm$, $h3 = 2.00mm$)

suggest that this method of transition have a high tolerance level. Figure 5.5 shows the final prototype which had been manufactured. The dimensions were chosen such that the entire prototype is stable and measurements can be taken easily. Figure 5.6 shows the final proposed PCB design for manufacturing with coplanar to microstrip transition along with $25\mu m$ pullback and $15\mu m$ width reduction in either side of the PCB. One other issue which needed to be considered is the entire length of the prototype ($len3$). The maximum distance between the two GSG probes in the measurement setup is 20 mm. Hence while designing the prototype the total length was kept below 20mm ($len3=16.852$ mm).

All the simulations and optimised results which have been shown before have been done with Roger 3010 substrate having $\epsilon_r = 10.2$ using simulation software CST. However the available substrate for manufacture was alumina ($\epsilon_r = 9.9$). Figure 5.7 shows the simulated results for the final prototype and PCB ($25\mu m$ 'pullback' and $15\mu m$ gap) for both these substrates. These results have been obtained using frequency domain solver in CST. As seen in the figure changing the substrate with a slightly different ϵ_r doesn't affect the return loss to a high extent. The bandwidth of the transition also remains the same as before (21.14 %). The final result for the back to back transition obtained for alumina had also been verified using simulation software HFSS. As seen in figure 5.7 the results obtained using these two software are similar with a slight variation which was due to the different methods in which the coplanar mode is excited by the waveguide ports in these two software.

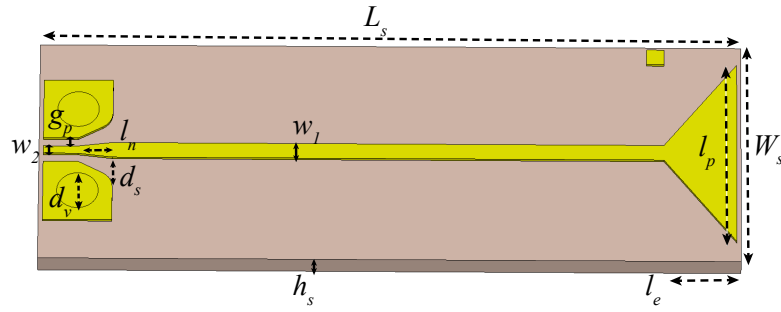


Figure 5.6: Final PCB Design with Coplanar-Microstrip transition included ($L_s = 4.025\text{mm}$, $W_s = 1.47\text{mm}$, $l_p = 1.215\text{mm}$, $l_e = 0.42\text{mm}$, $h_s = 0.127\text{mm}$, $w_1 = 0.1\text{mm}$, $w_2 = 0.05\text{mm}$, $g_p = 0.055\text{mm}$, $d_v = 0.24\text{mm}$, $d_s = 0.175\text{mm}$, $l_n = 0.2\text{mm}$).

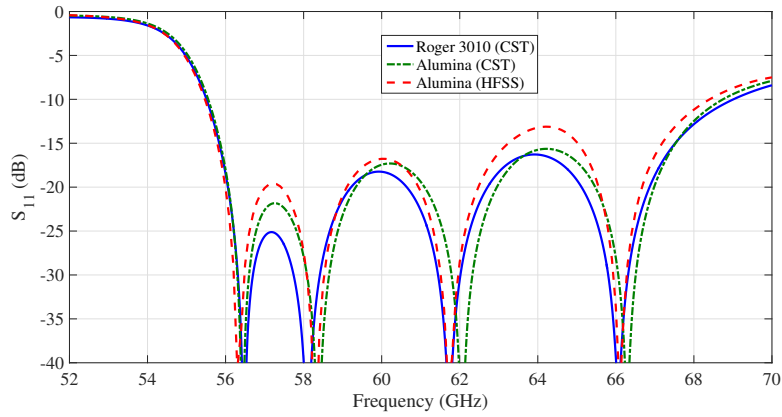


Figure 5.7: Simulated S parameters for the final prototype of RGW to microstrip transition for Roger 3010 and Alumina and results verified using HFSS.

5.2 Simulated Results for GGW

In this section transition from rectangular waveguide to GGW is discussed as the GGW had to be excited with WR-15 waveguide flange. This transition had been added to the previously optimised GGW to microstrip transition and its results are presented and discussed. The final prototype of the structure is also presented.

5.2.1 Rectangular Waveguide to GGW Transition

Figure 5.8 shows the transition from Rectangular waveguide to GGW along with the optimised value of the transition. The length of the Groove and the rectangular waveguide are equal (3.8 mm). The difference is in the width (rectangular waveguide width = 1.9 mm and groove width = 1.5 mm). The tuning parameters used to get the best possible return loss are 'h1', 'h2' and 'len'. As seen from the figure the optimised value of $len = 1.45 \sim \lambda/4$. The optimised result have a very good return loss below 20 dB as seen in figure 5.9.

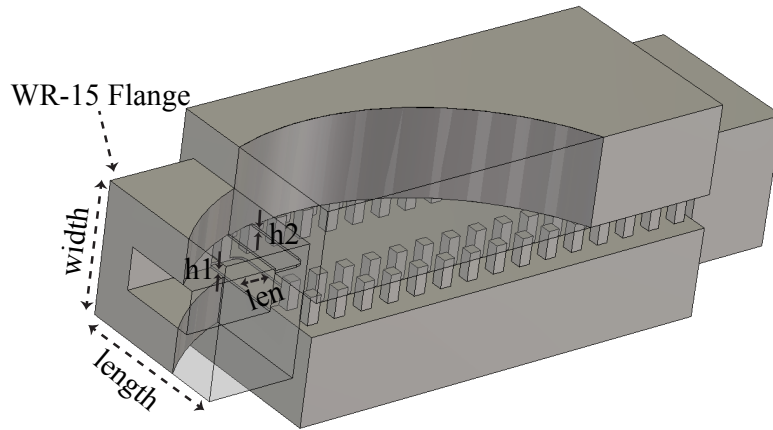


Figure 5.8: Back to back transition from rectangular to GGW. ($width = 1.9mm$, $length = 3.8mm$, $h1 = 0.1mm$, $h2 = 0.1mm$, $len = 1.45mm$)

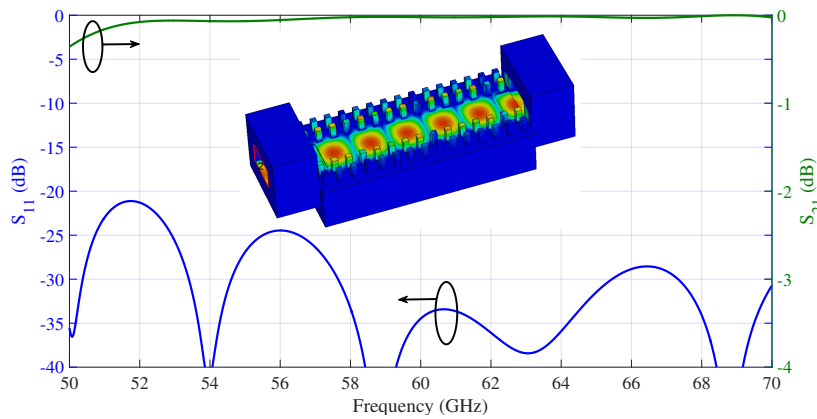


Figure 5.9: S parameters for back to back transition for rectangular to GGW.

5.2.2 Final Prototype (GGW) and Simulated Results

Including the above optimised back to back transition from rectangular waveguide to GGW to the previously optimised transition from GGW to microstrip, the S parameters obtained is shown in figure 5.10. The first plot shows the return loss for GGW to microstrip transition without rectangular waveguide excitation and the second plot shows the retrun loss for transition including the rectangular waveguide excitation. Finally as done previously for the RGW transition a pullback of $25 \mu m$ and a gap of $15 \mu m$ is included in the PCB (return loss shown in the third plot). As seen from these plots, there is slight change in the S parameters and the return loss is better than 15 dB for the entire band.

Figure 5.11 show the final proposed PCB design for manufacturing. Figure 5.12 shows the final manufactured prototype for the GGW to microstrip transition with the PCB inside the prototype. The dimensions are chosen such that it is compatible for connecting the WR-15 flange to transfer signal to the GGW. The S parameters of the final prototype is shown in figure 5.13. As mentioned earlier that Alumina ($\epsilon_r = 9.9$) was used for manufacture instead of Roger 3010 ($\epsilon_r = 10.2$). The optimization of the structure was done using CST Time Domain Solver and finally verified using

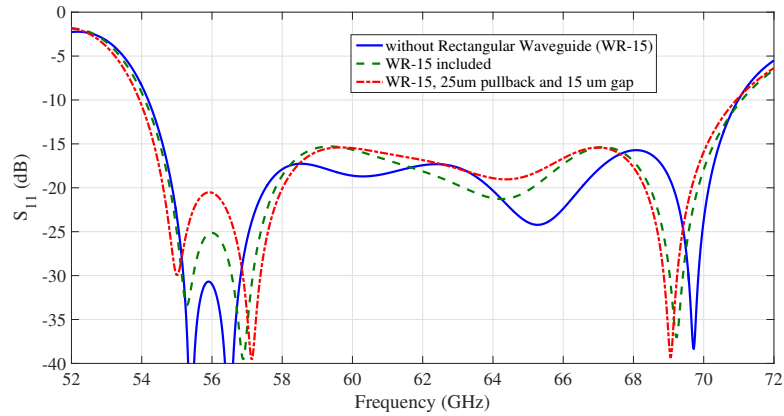


Figure 5.10: S parameters for back to back transition for GGW to Microstrip with additional transitions and PCB modified to comply with manufacturing specification and taking measurements.

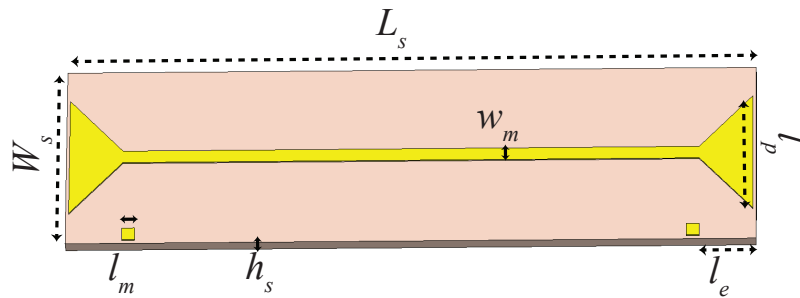


Figure 5.11: Final PCB design for GGW to microstrip transition including $25\mu\text{m}$ pullback and $30\mu\text{m}$ width reduction ($L_s = 5.458\text{mm}$, $W_s = 1.49\text{mm}$, $h_s = 0.127\text{mm}$, $l_e = 0.449\text{mm}$, $l_m = 0.1\text{mm}$, $w_m = 0.1\text{mm}$, $l_p = 0.977\text{mm}$)

CST Frequency Domain Solver and HFSS. As it can be seen from the figure there is a slight change in the S parameter when the substrate is changed from Roger 3010 to Alumina (first and second plot using CST- Time Domain Solver).

However, when the results are verified using CST Frequency Domain Solver and HFSS both have similar results (third and fourth curve) but there is a significant change when compared to the result obtained using the time domain solver in CST. This is due to the fact that the Time Domain Solver in CST uses Finite Integral Technique (FIT) where as Frequency Domain Solver in CST and HFSS uses Finite Element Method (FEM) with adaptive meshing. As the technique used by this two methods are different we observe a change in the results. The difference in solution is also due to the fact that adaptive meshing was not used for Time Domain Solver as it is very time consuming and hence not suitable for optimizing structures.

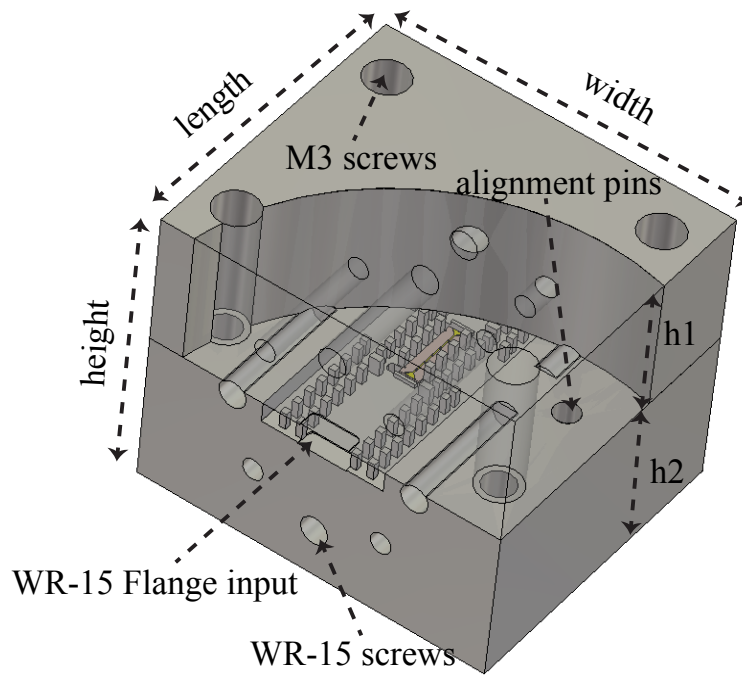


Figure 5.12: Final Prototype for GGW to Microstrip Transition ($length = 24.19mm$, $width = 27.6mm$, $height = 21.5mm$, $h1 = 10.0mm$, $h2 = 11.5mm$)

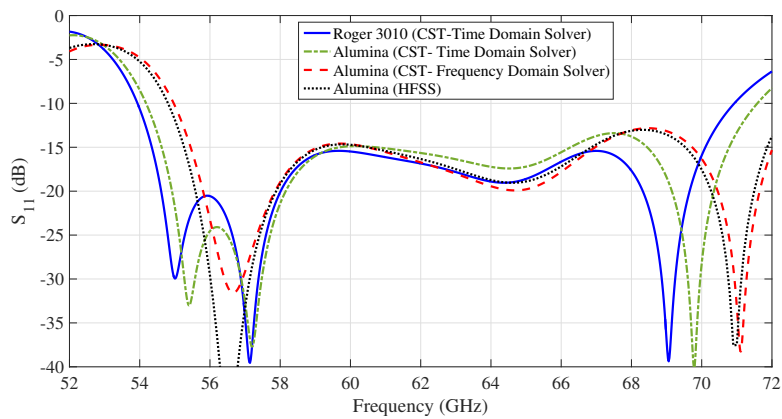


Figure 5.13: Simulated S parameters for the final prototype of GGW to microstrip transition for Roger 3010 and Alumina and results verified using HFSS.

As seen by the verified results of frequency domain solver in CST and HFSS there is a slight shift in the S parameters toward higher frequency and there is slightly a higher return loss (12.5 dB) at 69 GHz but have a good matching (return loss better than 10 dB) even beyond 72 GHz (approximately 73 GHz).

6

Measured Results

In this chapter the measured results for the manufactured prototypes for RGW and GGW is presented and compared with the simulation results. The deviation of the measured results from the simulated results is also look into and possible explanation for such deviation is presented. The prototypes for both the RGW and GGW transitions were manufactured in brass prototypes so that the PCB could be soldered on the prototypes. These prototypes were manufactured by using a computer numerical control (CNC) milling machine. The best quality milling machine can give an accuracy of $\pm 1\mu m$ in the horizontal direction and slightly more than $\pm 1\mu m$ in the vertical direction. The PCBs were manufactured using standard photolithography process. Since the PCB needed to be soldered to the prototype the bottom plate of the PCB was made solderable using $0.5\mu m$ of gold. The dimensions of the etched strip and the gaps between them have a tolerance of $\pm 2.54\mu m$ and the dicing of the substrate can be hold upto $\pm 25.4\mu m$.

6.1 Measurd Results for RGW

6.1.1 Manufactured Prototypes and PCB

Figure 6.1 and 6.2 shows the manufactured prototype for the RGW and the manufactured PCB respectively. The via holes of the GSG pads for the coplanar waveguide of the PCB have been realised using laser drilling and gold-plated. The tolerance level of the hole diameter and hole location is about $\pm 51\mu m$. The dimensions of both the prototype and the PCB have been checked in the microscope and presented



Figure 6.1: Manufactured prototype of RGW with PCBs integrated in the transition region.

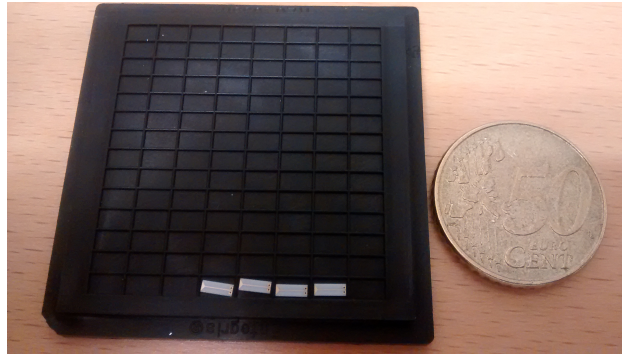


Figure 6.2: Manufactured PCB for RGW.

Table 6.1: Comparison between required and manufactured dimensions for RGW prototype (wrt figure 4.5)

Dim. (mm)	Required	Port 1	Port 2	Average Error
l_c	2.723	2.531	2.468	~ -0.233
w_c	0.843	0.759	0.713	~ -0.107
d_c	1.188	0.992	0.989	~ -0.198
h_1	0.487	0.486	0.517	$\sim +0.008$
h_2	1.013	1.010	1.038	$\sim +0.007$
h_3	1.250	1.268	1.290	$\sim +0.030$
l_1	1.256	1.216	1.273	$\sim +0.011$
l_2	0.916	0.903	0.894	$\sim +0.018$

in tables 6.1 and 6.2. The transition was also put to some initial tolerance test and it was observed through simulation that the S parameters are in acceptable level even upto $\pm 50\mu m$. This is in fact really high tolerance level in terms to millimeter wave transition. As seen in table 6.1 few of the dimensions for the RGW prototype are way out of the acceptable tolerance level and some dimensions of the manufactured prototype have errors going upto $\pm 200\mu m$ (indicated in red). The PCB for the RGW is at the acceptable tolerance level as seen in table 6.2.

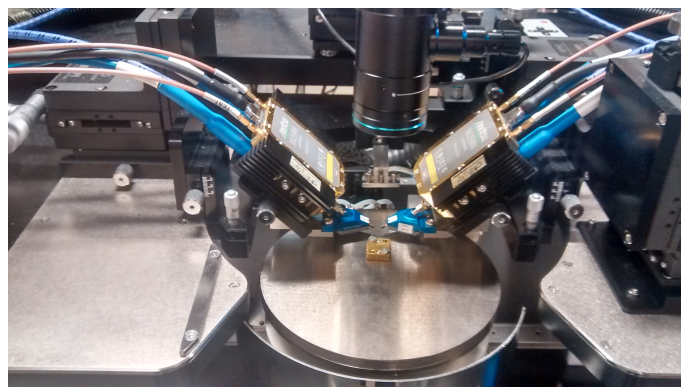
6.1.2 Experimental Setup and Measurements

Figure 6.3 shows the measurement setup for taking measurements for the RGW transition. It consists of two GSG probes which can be adjusted so it touches the coplanar pads of the PCBs. Before taking the measurements calibration was done using TRRL calibration method using a standard wafer available for calibration. However, more better calibration could be done where the entire effect of the coplanar pads of the PCB could be cancelled but for that additional TRL PCB lines had to be manufactured and due to cost constrains it was avoided. Figure 6.4 shows the return and insertion loss for one of the ports and compared to the simulated results. Whereas, figure 6.5 shows the S parameters for both the ports. As seen in the figures the results obtained are not very promising. The first reason for this is the faulty manufacturing process where some dimensions have error even upto $\pm 200\mu m$. Due to the less tolerance of the manufacturing process the PCBs could

Table 6.2: Comparison between required and manufactured dimensions for RGW chip (wrt figure 5.6)

Dim. (mm)	Required	Manufactured	Approx. Error
h_s	0.127	0.137	$\sim +0.010$
l_e	0.420	0.416	~ -0.004
W_s	1.470	1.466	~ -0.004
L_s	4.025	4.051	$\sim +0.026$
l_p	1.215	1.207	~ -0.008
w_1	0.100	0.100	~ -0.000
w_2	0.050	0.050	~ -0.000
g_p	0.055	0.055	~ -0.000
d_v	0.240	0.236	~ -0.004

not be placed initially into the structure and the pins adjacent to the PCB had to be milled out by $25\mu m$ in order to place the PCB. However there were some traces of the metal pieces left due to which the PCBs could not fit well into the structure. Hence there were lots of miss alignment errors even upto $100\mu m$. And since there were two PCBs this miss alignment error had sever effect on the performance. This miss alignment error is also shows in figure 6.5 due to which the return loss for the two ports are dissimilar. One expected result is that at frequencies where the return loss is below 10 dB the insertion loss should be better than 1 dB. However, this is not the case and the best possible insertion loss is around 5 dB. The reason for this could be the leakage of signals through parallel plate modes between the prototype and the ground plane of the PCB. Furthermore it is quite challenging to take measurements using GSG probe setup and the repeatability factor is also not very impressive with such device. However, this is only one result taken and the S parameters could be improved by trying to remove the traces to metals and placing the PCB more accurately into the prototype.

**Figure 6.3:** Measurement setup for taking measurement for RGW using GSG probe station.

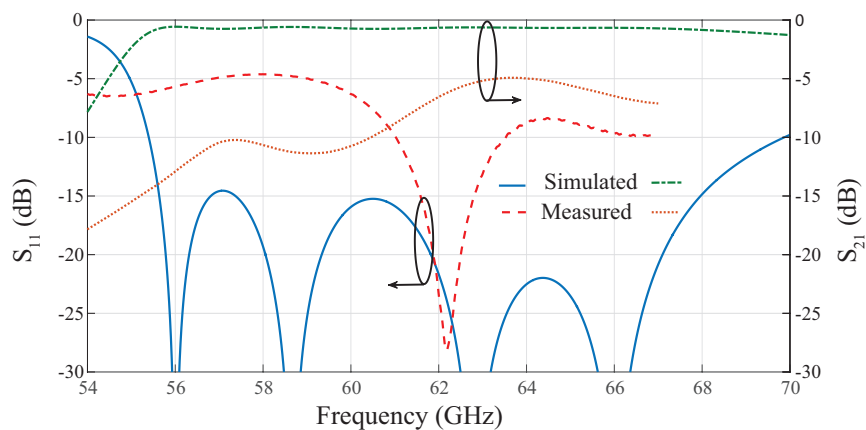


Figure 6.4: Measured S parameters for Port 1 and compared to simulated results

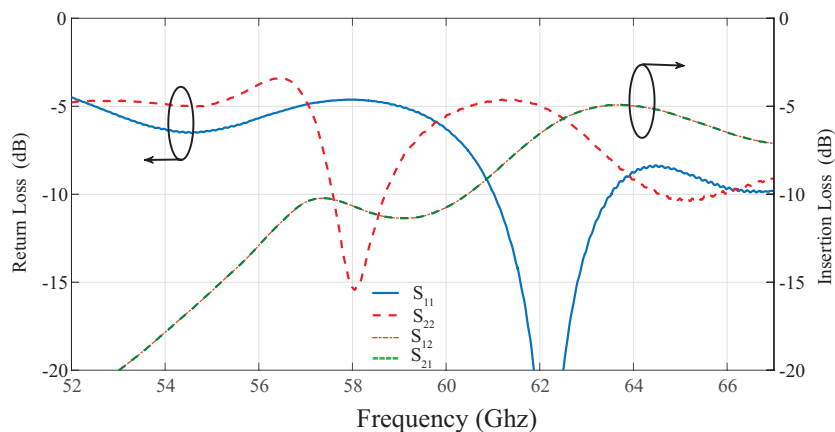


Figure 6.5: Measured S parameters for both the ports of the RGW transition.

6.2 Measured Results for GGW

6.2.1 Manufactured Prototypes and PCB

Figure 6.6 and 6.7 shows the manufactured prototype for the GGW and the PCB respectively. Some simulations had been done in order to check the tolerance level of the structure and it showed even $\pm 50\mu m$ error in the dimensions or placing of the PCB gave reasonable results for the transition. Table 6.3 and 6.4 shows the manufactured dimensions of the prototype and the PCB respectively. As seen in table 6.3 the dimensions of the cavity is smaller by about $\pm 200\mu m$. Hence, it was concluded that the manufacturing CNC machine was not of very high quality. The manufactured PCB seemed to be in the desired dimensions which are presented in table 6.4.

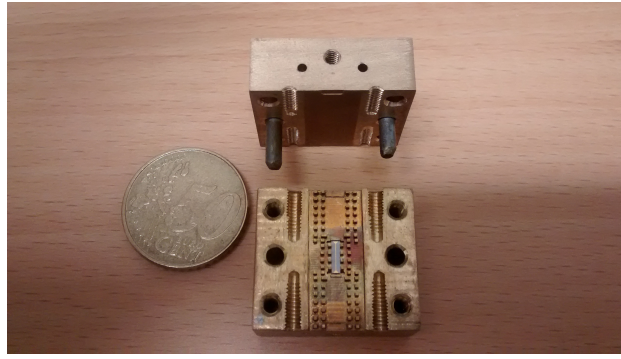


Figure 6.6: Manufactured prototype of GGW with PCBs integrated in the transition region.

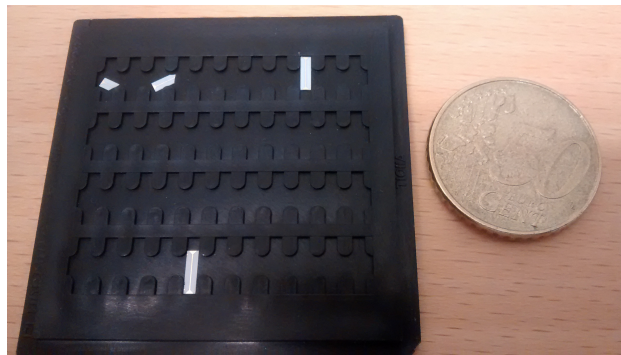


Figure 6.7: Manufactured PCB for GGW.

6.2.2 Experimental Setup and Measurements

Figure 6.8 shows the experimental setup for taking measurements for the GGW transition. As it can be seen in the figure the transition is excited using a WR-15 waveguide flange which is connected to extender. The work of the extender is to convert the signal received from the Vector Network Analyser (VNA) to frequencies upto V-Band. Initially before taking the measurements the entire measurement setup had been calibrated using the standard calibration kit available for the setup. After calibration the measurement setup had return loss below 50 dB when the two WR-15 flange were connected together. First measurement taken in order to check if there is any leakage of signals between the ports or is there is any sort of resonance in the structure. Figure 6.9 shows the measured result without integrating the PCB into the prototype. As it can be seen in the figure the insertion loss is below 60 dB and the return loss is around 0.5 dB. This proves that the S parameters received by placing the PCB will solely be due to the transition and not due to resonance or leakage. Due to the less manufacturing tolerance of the prototype the region in which the PCB had to be placed was slightly smaller even after reducing the PCB width by $\pm 15\mu m$ on each side. Hence the pins where the PCB had to be placed were milled out by $\pm 25\mu m$. Figure 6.10 shows the result obtained after integrating the PCB on the prototype. As seen in the figure the return loss is better than 10 dB from 57 to 74 GHz and the insertion loss in this band is around 1 dB which is more than the insertion loss got through simulation (0.5 dB). This is because PEC

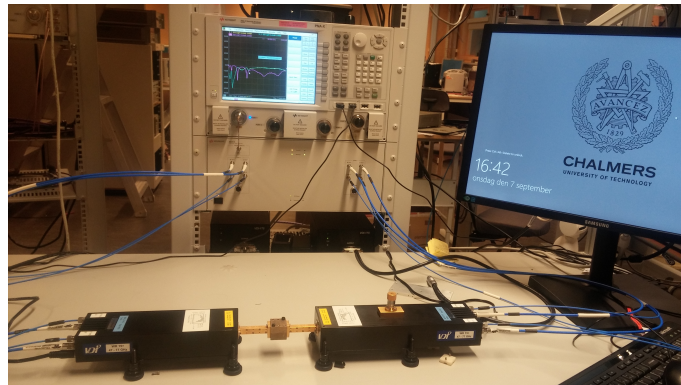
Table 6.3: Comparison between required and manufactured dimensions for GW prototype (wrt figure 4.14)

Dim. (mm)	Required	Port 1	Port 2	Average Error
l_c	3.389	3.112	3.134	~ -0.269
w_c	0.728	0.604	0.588	~ -0.133
d_c	0.912	0.850	0.856	~ -0.059
w_b	0.239	0.308	0.385	$\sim +0.111$
h_b	0.305	0.317	0.316	$\sim +0.011$
l_b	1.690	1.756	1.836	$\sim +0.100$
e_p	0.367	0.463	0.439	$\sim +0.083$
e_c	0.387	0.410	0.457	$\sim +0.050$

Table 6.4: Comparison between required and manufactured dimensions for GW chip (wrt figure 5.11)

Dim. (mm)	Required	Manufactured	Approx. Error
h_s	0.127	0.130	$\sim +0.003$
l_e	0.424	0.422	~ -0.002
W_s	1.490	1.482	~ -0.008
L_s	5.458	5.449	~ -0.009
l_p	0.977	0.970	~ -0.007

was used instead of brass for the simulation model and hence the additional 0.5 dB loss is due to the losses in the brass prototype. This is also confirmed through the measured results in figure 6.9 which have return loss of 0.5 dB without the PCB. The measured results also shows that the band for the transition region has shifted by 2 GHz. This is due to the faulty manufactured prototype in which the cavity dimensions have been made smaller than required. There are also some ripples in the measured return loss which is suspected to be due to air gap between the surface of the prototype and the ground plane of the PCB which leads to the leakage of signals through parallel plate modes. It is also to be noted that the repeatability factor for

**Figure 6.8:** Measurement setup for taking measurement for GW using WR-15 Flange.

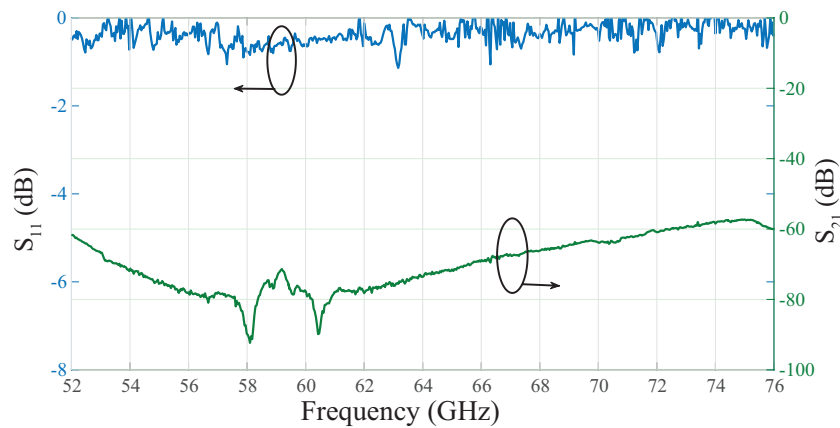


Figure 6.9: Measured S parameters for no PCB integrated in the transition region.

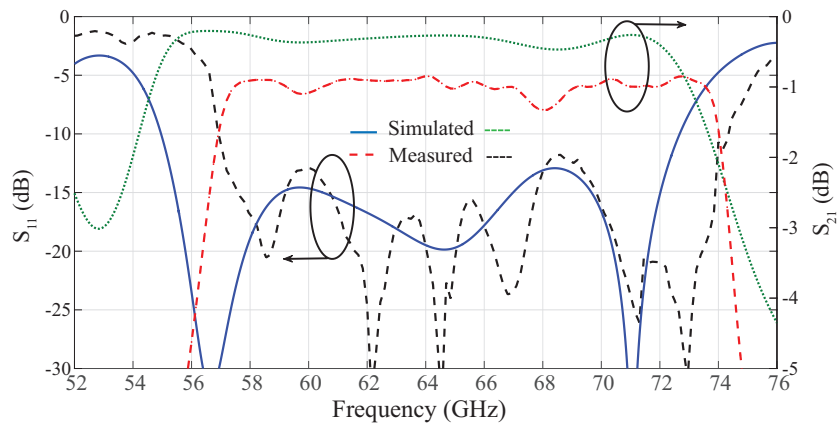


Figure 6.10: Measured S parameters for PCB placed in the transition region through soldering.

the measurements highly depends upon how well the PCB have been integrated to the prototype. The results presented here is the best result obtained after several tries for proper alignment of the PCB into the structure.

7

Conclusion and Future Work

A new technique to make contactless transition from microstrip to Gap waveguide using backshort cavity method have been developed. The transition for RGW due to faulty manufacturing and high assembling error didn't give reasonable S parameters as expected through simulations. However, the transition for the GGW gave results which were similar to simulated results with 2 GHz shift in the frequency band due to manufacturing error. The measured results thus validates the working of such kind of transition technique.

The next part of this project is to use this transition in the feed-network and integrate MMIC chips (Tx/Rx, Power Amplifiers, Phase shifters etc.) with gap waveguide array antennas. However, there are still lots of challenges which needs to be overcome in order to integrate MMIC chips with gap waveguide antennas. Figure 7.1 shows a manufactured 8 by 8 RGW array antenna consisting of three layers feed network layer, cavity layer and the slot layer. The rectangular box in the feed layer shows the possible location where the MMIC chips could be integrated. The dimensions of these possible location is $6mm \times 3mm$. However the entire transition including the steps in the ridge requires about $10mm \times 3mm$ area. Hence the length of the transition is bigger than the available space. Also there should be minimum of one pin between the MMIC chip and the radiating slot to avoid any sort of coupling of signals. Hence the feed network of the array antenna needs to be modified so that it could include the transition region. Then smart design technique also needs to be done in order to have the DC bias for the MMIC chips.

In this project the transition were made keeping in mind that it had to be integrated in the feed network of the gap waveguide antenna. Hence the transition required to be compact and occupy less space as possible. However, if there is no space constrain it is possible to achieve very high bandwidth which goes upto even 40% using elliptical cavity instead of rectangular cavity. The measured results proves the working of this kind of transitions and hence we conclude that similar transition could also be designed for rectangular waveguide-microstrip and microstrip-microstrip transitions. Conventional rectangular waveguide- microstrip transitions using backshort have bandwidth of around 30% and the microstrip is in the perpendicular plane to that of the rectangular waveguide. This transition technique could be used to achieve higher bandwidth and RF circuits could be integrated inside the rectangular waveguide in the plain of the waveguide walls. The microstrip-microstrip transition have the potential to replace the old traditional methods to making chip to chip transitions through flip-chip and bond wires. Figure 7.2 shows the conventional method

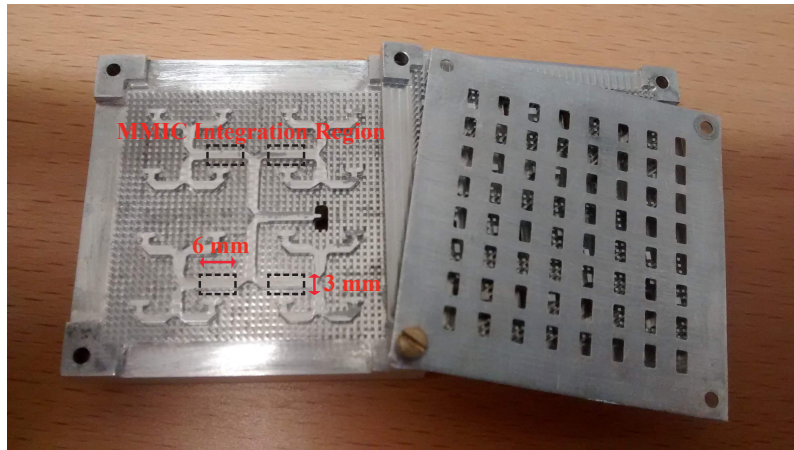


Figure 7.1: RGW Array Antenna with rectangles indicating the possible positions where the MMIC can be integrated.

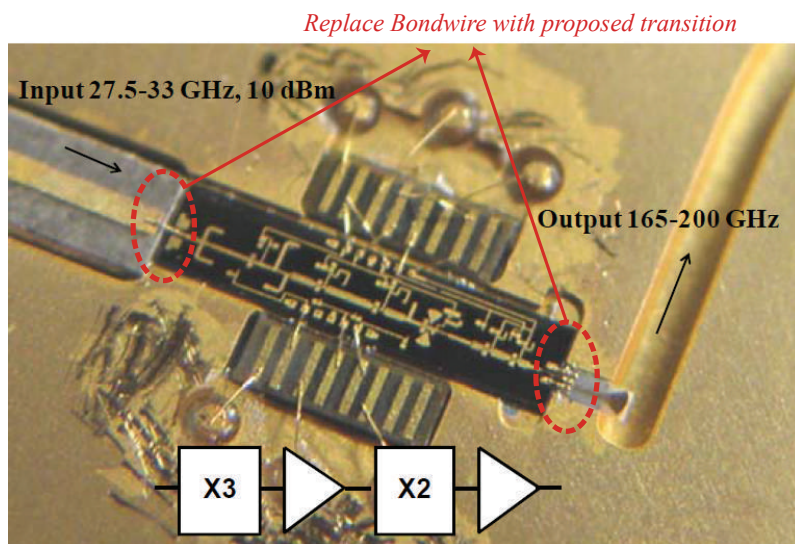


Figure 7.2: Conventional method of making transition from MMIC using bondwires which can be replaced with back short cavity transition technique.

in which transitions from MMIC and other RF circuits are done using bond-wires. There are several issues with bond wire transitions which had been addressed in the introduction. This new transition technique can be used to replace this old traditional method of bond-wires. Hence this open up several areas in which this kind of transition technique can be used and further investigations needs to be done.

Bibliography

- [1] Emerson, D. T. "*The work of Jagadis Chandra Bose: 100 years of mm-wave research.*" IEEE Transactions on Microwave Theory and Techniques 45.12 (1997).
- [2] Ramminger, S., N. Seliger, and G. Wachutka. "*Reliability model for Al wire bonds subjected to heel crack failures.*" Microelectronics Reliability 40.8 (2000): 1521-1525.
- [3] Sutono, Albert, et al. "*Experimental modeling, repeatability investigation and optimization of microwave bond wire interconnects.*" Advanced Packaging, IEEE Transactions on 24.4 (2001): 595-603.
- [4] Chen, Jian, et al. "*Mechanical issues of Cu-to-Cu wire bonding.*" Components and Packaging Technologies, IEEE Transactions on 27.3 (2004): 539-545.
- [5] Wang, Chin-Te, et al. "*Investigation of the Flip-Chip Package With BCB Underfill for W-Band Applications.*" Microwave and Wireless Components Letters, IEEE 24.1 (2014): 11-13.
- [6] Burke, John J., and Robert W. Jackson. "*Surface-to-surface transition via electromagnetic coupling of microstrip and coplanar waveguide.*" Microwave Theory and Techniques, IEEE Transactions on 37.3 (1989): 519-525.
- [7] Strauss, Georg, and Wolfgang Menzel. "*Millimeter-wave MMIC interconnects using electromagnetic field coupling.*" Electrical Performance of Electronic packaging, 1994., IEEE 3rd Topical Meeting on. IEEE, 1994.
- [8] Strauss, Georg, and Wolfgang S. Menzel. "*Millimeter-wave monolithic integrated circuit interconnects using electromagnetic field coupling.*" Components, Packaging, and Manufacturing Technology, Part B: Advanced Packaging, IEEE Transactions on 19.2 (1996): 278-282.
- [9] Ellis, Thomas J., et al. "*A wideband CPW-to-microstrip transition for millimeter-wave packaging.*" Microwave Symposium Digest, 1999 IEEE MTT-S International. Vol. 2. IEEE, 1999.
- [10] Vassilev, Vessen, et al. "*Integrated front-ends up to 200 GHz.*" Microwave Workshop Series on Millimeter Wave Integration Technologies (IMWS), 2011 IEEE MTT-S International. IEEE, 2011.
- [11] Zaman, Ashraf Uz. *Gap waveguide: Low loss microwave passive components and MMIC packaging technique for high frequency applications.* Chalmers University of Technology, 2013.
- [12] Rajo-Iglesias, Eva, Ashraf Uz Zaman, and Per-Simon Kildal. "*Parallel plate cavity mode suppression in microstrip circuit packages using a lid of nails.*" Microwave and Wireless Components Letters, IEEE 20.1 (2010): 31-33.
- [13] Yong, Su Khiong, and Chia-Chin Chong. "*An overview of multigigabit wireless through millimeter wave technology: potentials and technical challenges.*"

- EURASIP Journal on Wireless Communications and Networking 2007.1 (2006): 1-10.
- [14] Roh, Wonil, et al. *"Millimeter-wave beamforming as an enabling technology for 5G cellular communications: theoretical feasibility and prototype results."* Communications Magazine, IEEE 52.2 (2014): 106-113.
- [15] Sievenpiper, Dan, et al. *"High-impedance electromagnetic surfaces with a forbidden frequency band."* Microwave Theory and Techniques, IEEE Transactions on 47.11 (1999): 2059-2074.
- [16] Kildal, Per-Simon, et al. *"Local metamaterial-based waveguides in gaps between parallel metal plates."* Antennas and Wireless Propagation Letters, IEEE 8 (2009): 84-87.
- [17] Kildal, Per-Simon, et al. *"Design and experimental verification of ridge gap waveguide in bed of nails for parallel-plate mode suppression."* Microwaves, Antennas & Propagation, IET 5.3 (2011): 262-270.
- [18] Kildal, Per-Simon. *"Artificially soft and hard surfaces in electromagnetics."* Antennas and Propagation, IEEE Transactions on 38.10 (1990): 1537-1544.
- [19] Rajo-Iglesias, Eva, and Per-Simon Kildal. *"Numerical studies of bandwidth of parallel-plate cut-off realised by a bed of nails, corrugations and mushroom-type electromagnetic bandgap for use in gap waveguides."* Microwaves, Antennas & Propagation, IET 5.3 (2011): 282-289.
- [20] Valero-Nogueira, Alejandro, et al. *"Experimental demonstration of local quasi-TEM gap modes in single-hard-wall waveguides."* Microwave and Wireless Components Letters, IEEE 19.9 (2009): 536-538.
- [21] Rajo-Iglesias, Eva, and Per-Simon Kildal. *"Groove gap waveguide: A rectangular waveguide between contactless metal plates enabled by parallel-plate cut-off."* Antennas and Propagation (EuCAP), 2010 Proceedings of the Fourth European Conference on. IEEE, 2010.
- [22] Pucci, Elena, et al. *"New low loss inverted microstrip line using gap waveguide technology for slot antenna applications."* Antennas and Propagation (EuCAP), Proceedings of the 5th European Conference on. IEEE, 2011.
- [23] Vosoogh, Abbas, and Per-Simon Kildal. *"Corporate-fed planar 60 GHz slot array made of three unconnected metal layers using AMC pin surface for the gap waveguide."* (2015).
- [24] Vosoogh, Abbas, Per-Simon Kildal, and Vessen Vassilev. *"A multi-layer gap waveguide array antenna suitable for manufactured by die-sink EDM."* 2016 10th European Conference on Antennas and Propagation (EuCAP). IEEE, 2016.
- [25] Leong, Yoke-Choy, and Sander Weinreb. *"Full band waveguide-to-microstrip probe transitions."* Microwave Symposium Digest, 1999 IEEE MTT-S International. Vol. 4. IEEE, 1999.
- [26] Risacher, Christophe, et al. *"Waveguide-to-microstrip transition with integrated bias-T."* Microwave and Wireless Components Letters, IEEE 13.7 (2003): 262-264.
- [27] Sakakibara, Kunio. *Broadband and Planar Microstrip-to-waveguide Transitions.* INTECH Open Access Publisher, 2010.

-
- [28] Yao, Hui-Wen, et al. "*Analysis and design of microstrip-to-waveguide transitions.*" *Microwave Theory and Techniques, IEEE Transactions on* 42.12 (1994): 2371-2380.
- [29] Rebollo, Ainara, et al. "*Full W-Band microstrip-to-waveguide inline transition.*" *Antennas and Propagation (EuCAP), 2014 8th European Conference on.* IEEE, 2014.
- [30] Kaneda, Noriaki, Yongxi Qian, and Tatsuo Itoh. "*A broad-band microstrip-to-waveguide transition using quasi-Yagi antenna.*" *Microwave Theory and Techniques, IEEE Transactions on* 47.12 (1999): 2562-2567.
- [31] Zaman, Ashraf Uz, et al. "*Design of a simple transition from microstrip to ridge gap waveguide suited for MMIC and antenna integration.*" *Antennas and Wireless Propagation Letters, IEEE* 12 (2013): 1558-1561.
- [32] Algaba Brazález, Astrid, Ashraf Uz Zaman, and Per-Simon Kildal. "*Investigation of a Microstrip-to-Ridge Gap Waveguide transition by electromagnetic coupling.*" *IEEE Antennas and Propagation Society, AP-S International Symposium (Digest).* 2012.
- [33] Brazález, Astrid Algaba, et al. "*Design of-Band Transition From Microstrip to Ridge Gap Waveguide Including Monte Carlo Assembly Tolerance Analysis.*" *IEEE Transactions on Microwave Theory and Techniques* 64.4 (2016): 1245-1254.
- [34] Alós, Esperanza Alfonso, Ashraf Uz Zaman, and Per-Simon Kildal. "*Ka-band gap waveguide coupled-resonator filter for radio link diplexer application.*" *IEEE Transactions on Components, Packaging and Manufacturing Technology* 3.5 (2013): 870-879.
- [35] Potok, M. H. N. "*Capacitive-iris-type mechanically tunable waveguide filters for the X-band.*" *Proceedings of the IEE-Part B: Electronic and Communication Engineering* 109.48 (1962): 505-510.